DEPARTMENT OF PHYSICS

The Catholic University of America

Washington, D.C. 20064

Modal and Surface Wave Resonances In Acoustic-Wave Scattering from Elastic Objects and in Elastic-Wave Scattering from Cavities

H. Überall

Department of Physics

Catholic University of America, Washington, D.C. 20064

Supported by the Office of Naval Research,

Physics Program Office, Code 421,

Under Contract No. ONR -

N00014-76-C-0430

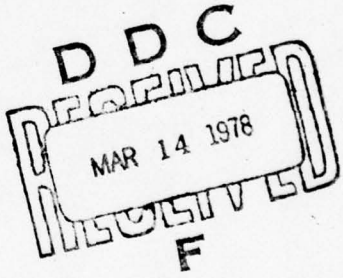

Unclassified

SECURITY CLASSIFICATION OF THIS PAGE (When Data Entered)

REPORT DOCUMENTATION PAGE

READ INSTRUCTIONS BEFORE COMPLETING FORM

1. REPORT NUMBER

2. GOVT ACCESSION NO.

3. RECIPIENT'S CATALOG NUMBER

4. TITLE (and Subtitle)

(6) MODAL AND SURFACE WAVE RESONANCES IN ACOUSTIC-WAVE SCATTERING FROM ELASTIC OBJECTS AND IN ELASTIC-WAVE SCATTERING FROM CAVITIES.

5. TYPE OF REPORT & PERIOD COVERED
Technical Report (interim)
Nov. 1, 1976-Oct. 31, 1977

6. PERFORMING ORG. REPORT NUMBER

7. AUTHOR(s)

(10) H. Überall

8. CONTRACT OR GRANT NUMBER(s)

(15) ONR
N00014-76-C-0430

9. PERFORMING ORGANIZATION NAME AND ADDRESS
Department of Physics
Catholic University of America
Washington, D.C. 20064

10. PROGRAM ELEMENT, PROJECT, TASK AREA & WORK UNIT NUMBERS
Program 61153N, Project RR011-08, Task RR011-08-01
Work Unit NR 384-914

11. CONTROLLING OFFICE NAME AND ADDRESS
Office of Naval Research
Physics Program Office
Arlington, V.A. 22217

(11) 21

12. REPORT DATE
Oct[illegible] 1977

13. NUMBER OF PAGES
38 pages, & 17 Figures

14. MONITORING AGENCY NAME & ADDRESS (if different from Controlling Office)

(9) Technical rept.
1 Nov 76-31 Oct 77

15. SECURITY CLASS. (of this report)
Unclassified

15a. DECLASSIFICATION/DOWNGRADING SCHEDULE

16. DISTRIBUTION STATEMENT (of this Report)

(16) RR011 08

Approved for public release; distribution unlimited

(12) 58p.

(17) RR011 08 01

17. DISTRIBUTION STATEMENT (of the abstract entered in Block 20, if different from Report)

18. SUPPLEMENTARY NOTES
Based on an invited paper delivered at the Sept. 12-15, 1977 IUTAM Symposium "Modern Problems in Elastic Wave Propagation", Northwestern University, Evanston, Illinois (J. Achenbach and J. Miklowitz, Organizers)

19. KEY WORDS (Continue on reverse side if necessary and identify by block number)
Acoustic Scattering; Elastic-Wave Scattering; Resonances of Elastic Objects; Resonances of Cavities; Breit-Wigner Resonances; Regge Poles; Eigenvibrations of Elastic Objects.

20. ABSTRACT (Continue on reverse side if necessary and identify by block number)

The problems of the scattering of waves from an obstacle, no matter in which field of physics they are being considered, exhibit an essential similarity. This similarity extends from the scattering of sound waves by an elastic object (acoustics) over elastic wave scattering from a cavity (geophysics and materials testing) to the problems of particle scattering from particles and nuclei (high energy and nuclear physics).

DD FORM 1 JAN 73 1473 EDITION OF 1 NOV 65 IS OBSOLETE
S/N 0102-LF-014-6601

Unclassified
SECURITY CLASSIFICATION OF THIS PAGE (When Data Entered)

Grant page

076433

AB

Block # 20

While historically, progress has been made along different lines in the various fields, it has become clear that more may be learned by applying the methods of one field of physics in another one, and vice versa, so that the basic similarities of the scattering problem may be exhibited and exploited. In this vein, after having studied surface wave phenomena in acoustic scattering by what is known in nuclear physics as Regge pole techniques, we apply the Breit-Wigner resonance scattering formalism of nuclear physics* to both acoustic and elastic wave scattering (essentially another way of exhibiting the Regge poles), and relate the resonances to the eigenvibrations of the scattering object.

* is applied

Contents

Introduction

The results reported in this paper have been obtained in collaboration with many colleagues and students, and it is difficult for me to give adequate justice to their enthusiastic and dedicated work. The least I may do here is to list their contributions and have their generous help acknowledged by name, as follows:

Acoustic Wave Scattering from Elastic Cylinders and Spheres:

Dr. Joseph W. Dickey (NSRDC, Annapolis): Surface Wave Resonances

Dr. Larry Flax, Mr. Louis R. Dragonette (NRL, Washington): Breit-Wigner Resonances

Dr. Jacob George (Catholic University): Resonances in transmitted elastic waves

Acoustic Wave Scattering from Viscoelastic Spheres:

Dr. Guillermo C. Gaunaurd (NSWC White Oak), Dr. Larry Flax (NRL Washington)

Acoustic Wave Scattering from Elastic Cylindrical Shells:

Dr. J. Diarmuid Murphy (CUA), Mr. Edward D. Breitenbach (NSRDC Carderock)

Elastic Wave Scattering from Cylindrical Cavities:

Dr. Anton J. Haug (Johns Hopkins APL), Mr. Sheldon G. Solomon (NSRDC Carderock)

Elastic Wave Scattering from Spherical Cavities:

Dr. Guillermo C. Gaunaurd (NSWC White Oak)

It will be shown in the following that the variety of the mentioned scattering problems is essentially governed by very similar phenomena, namely the resonant excitation of the eigenvibrations of the scattering object, be that an elastic body subject to an incident acoustic wave, or a fluid-filled cavity in an elastic material exposed to compressional or shear waves. These resonances often occur over a quite narrow frequency interval (the width being proportional to the imaginary part of the complex eigenfrequency of the body while it is in contact with its surroundings), and in between the eigenfrequencies, the scatterer behaves as if it could not vibrate (the elastic object, e.g., as if it were rigid; the fluid-filled cavity as if it were empty). This behavior of the scattering object provides a continuous background to the scattering amplitude, upon which the resonances are superimposed, and with which they interfere in an often striking and unexpected manner.

When the scattering amplitude f is resolved into its usual normal modes f_n à la Rayleigh (also termed "partial waves"), the set of eigenfrequencies in the nth partial wave shifts to higher values as n is increased. The scattering amplitude may thus be considered a function of two (continuous) variables, ω and n, which for given n has a pole in the complex ω plane somewhat below the real ω-axis, i.e.

$$f_n(\omega) = A_n \frac{(\Gamma/2\pi)^{1/2}}{\omega - \omega(n) + \frac{1}{2} i \Gamma} \quad , \tag{1}$$

the pole being located at $\omega = \omega(n) - \frac{1}{2} i \Gamma$. The width Γ of the resonance is determined by the distance of the pole below the real axis, $\frac{1}{2}\Gamma$ (> 0). For a fixed frequency ω, $f_n(\omega)$ may be considered a function of n, and one may expand

$$\omega(n) \cong \omega(n_\omega) + (n - n_\omega)\omega'(n_\omega) \qquad (\omega' > 0), \tag{2}$$

where one chooses n_ω so that $\omega(n_\omega) = \omega$, i.e. the fixed incident frequency lies at the resonance peak when $n = n_\omega$. Then, the amplitude

$$f_n(\omega) = \frac{-A_n}{[\omega'(n_\omega)]^{1/2}} \frac{(\hat{\Gamma}/2\pi)^{1/2}}{n - n_\omega - \frac{1}{2} i \hat{\Gamma}} \tag{3}$$

appears with a pole in the complex n-plane, located at $n = n_\omega + \frac{1}{2} i \hat{\Gamma}$ above the real n-axis since

$$\hat{\Gamma} \equiv \Gamma / \omega'(n_\omega) > 0. \tag{4}$$

In terms of the n-variable, this is known as a Regge pole[1], and it shows that one and the same pole of the scattering amplitude may appear as a resonance in the ω as well as in the n variable. If n is considered a parameter and ω the variable, the n dependence of the resonance frequency $\omega(n)$

in Eq. (1) causes a "Regge recurrence" of the one Regge pole under consideration in all successive partial waves at successively higher resonance frequencies, as will be demonstrated in Sections 2 and further. In the following section, however, we shall discuss the Regge pole aspects of the scattering amplitude, Eq. (3), as it provides a physical picture of the scattering process in terms of surface waves ("creeping" or "circumferential waves"), as well a physical explanation of the mechanism of resonance excitation.

I. Surface Waves in Acoustic Scattering from an Elastic Cylinder

1) The Watson Transformation

An infinite plane acoustic wave $\exp i(kx - \omega t)$ of propagation constant $k = \omega/c$, incident along the x axis on a solid elastic cylinder of radius a, produces at the position (r, φ) of an observer located outside of the cylinder the total field

$$p = \sum_{n=0}^{\infty} \varepsilon_n i^n (B_n / D_n) \cos n\varphi \tag{5a}$$

where $\varepsilon_n = 1$ $(n = 0)$, $2 (n > 0)$. The quantity

$$B_n = D_n J_n(kr) + b_n H_n^{(1)}(kr) \tag{5b}$$

includes contributions from the incident ($\propto J_n$) and the scattered wave ($\propto H_n^{(1)}$). The 3 x 3 determinants b_n and D_n, given in the literature[2,3], contain cylinder functions with arguments $x \equiv ka = \omega a/c$, $x_L \equiv k_L a = \omega a/c_L$ and $x_T \equiv k_T a = \omega a/c_T$, where c_L, c_T are the velocities of longitudinal (compressional) and transverse (shear) waves in the cylinder (of density ρ_c) respectively, given by

$$c_L^2 = (\lambda + 2\mu)/\rho_c, \qquad c_T^2 = \mu/\rho_c \tag{5c}$$

which depend on the Lamé elastic constants λ and μ.

Eq. (5a) is called the Rayleigh or normal mode series of the scattering amplitude. It may be rewritten as a contour integral by means of the Watson transformation[2]

$$\sum_{n=0}^{\infty} \varepsilon_n f_n(x) = i P \oint_C \frac{d\nu}{\sin \pi\nu} e^{-i\pi\nu} f_\nu(x), \tag{6}$$

(P denoting the principal value at $\nu = 0$), where the contour C surrounds tightly on the both sides the positive real axis in the ν plane, and hence also the poles of the integrand at the integers $\nu = n$ which are caused by the factor $1/\sin\pi\nu$.

The amplitude f_ν , however, also has "Regge" poles located at complex positions $\nu = \nu_\ell$ ($\ell = 1, 2, \ldots$) in the first quadrant of the ν-plane, as indicated in Eq. (3) if we replace $n \to \nu$. The contour C may then be opened up to comprise infinite portions C_∞ on which the integral can be shown to vanish, as well as two finite portions C_o and C' as shown in Fig. 1, with C_o surrounding the poles of f_n. One then has for the scattered field

$$p = p_I + p_{II} \tag{7}$$

where

$$p_{II} = \frac{1}{2} i P \int_{C_o} \frac{d\nu}{\sin\pi\nu} e^{-i\nu\pi/2} \left[1 + \frac{2b_\nu}{D_\nu} \right] H_\nu^{(1)}(kr) \cos\nu\varphi, \tag{8}$$

the contribution from the term $\propto H_n^{(2)}$ in Eq. (5b) having vanished. The contribution of the "background integral" p_I, similar to Eq. (8) but led over the contour C' , has been shown to be small [3] and will be neglected.

The Regge poles $\nu = \nu_\ell$ of f_ν , Eq. (3), are determined

by the zeros of D_ν. For the case of the aluminum cylinder in water, these are shown schematically at some given frequency, in Fig. 2, with classification labels to be discussed later on. Splitting p_{II} into integrals over contours C_1 and C_2 (separated by a saddle point ν_s (see below), and applying Imai's transformation[2]

$$\cos\nu\varphi = e^{i\nu\pi}\cos\nu(\varphi-\pi) - i\,e^{i\nu(\pi-\varphi)}\sin\pi\nu \tag{9}$$

to the integral over C_2 serves to split off, via the second term of Eq. (9), a geometrical part p_g which no longer has $1/\sin\pi\nu$ in the integrand, and which will be evaluated at the saddle point ν_s of Fig. 2, resulting in the specularly reflected wave[2]. (Additional saddle points in p_g yield waves which are transmitted through the cylinder, see Reference 3.) The remaining integrals are evaluated in terms of the residues at the poles of Fig. 2, with the residue series converging on both the insonified and shadow sides of the cylinder[4].

We then have

$$p_{II} = p_g + p_r, \tag{10}$$

with a geometric contribution

$$p_g = \frac{1}{2}\int_{C_s} d\nu\, e^{i\nu(\frac{1}{2}\pi-\varphi)}\left[1 + \frac{2b_\nu}{D_\nu}\right] H_\nu^{(1)}(kr), \tag{10a}$$

and a residue contribution $p_r = p_1 + p_2$, split into two series

$$p_1 = -2\pi \sum_{\ell} \frac{\cos \nu_\ell \varphi}{\sin \pi \nu_\ell} e^{-i\nu_\ell \pi/2} \frac{b_{\nu_\ell}}{\dot{D}_{\nu_\ell}} H_{\nu_\ell}^{(1)}(kr), \qquad \mathrm{Re}\,\nu_\ell < \nu_s \ , \tag{10b}$$

$$p_2 = -2\pi \sum_{\ell} \frac{\cos \nu_\ell (\varphi - \pi)}{\sin \pi \nu_\ell} e^{i\nu_\ell \pi/2} \frac{b_{\nu_\ell}}{\dot{D}_{\nu_\ell}} H_{\nu_\ell}^{(1)}(kr), \qquad \mathrm{Re}\,\nu_\ell > \nu_s \ , \tag{10c}$$

where $\dot{D}_\nu = \partial D_\nu / \partial \nu$.

The expansion in e.g. Eq. (10b) of the quantity

$$\frac{\cos \nu_\ell \varphi}{\sin \pi \nu_\ell} = -i \sum_{\lambda = \pm 1} \sum_{m=0}^{\infty} e^{i\nu_\ell (\lambda \varphi + \pi + 2m\pi)} \ , \tag{11}$$

together with the time factor $\exp(-i\,\omega\, t)$ used by us shows that each residue has the factor

$$e^{i(\pm \nu_\ell \varphi - \omega t)} = e^{\mp \varphi\, \mathrm{Im}\,\nu_\ell}\, e^{i(\pm \varphi\, \mathrm{Re}\,\nu_\ell - \omega t)} \ , \tag{12}$$

which reveals it to be an attenuated circumferential wave, or "surface wave", with phase velocity

$$c_\ell = a\omega / \mathrm{Re}\,\nu_\ell \ . \tag{13}$$

Extensive numerical calculations of the positions of the zeros of D_ν, and of their trajectories (i.e. their motion through the complex ν-plane as one varies the value of x)

have been made by us earlier[5,6]. The results are shown schematically in Fig. 2; examples of scale plots of the zero positions are given elsewhere[7,8]. A series of "Franz (F) poles" $\nu = \nu_F$, all with large imaginary parts (i.e., high attenuations of the corresponding surface waves) lies along a curve starting at $\nu = x$ and reaching towards the upper right; a single "Stoneley (S) pole" ν_S with very small imaginary part (which tends towards the conventionally defined Stoneley pole[2,5] as $ka \to \infty$) lies slightly to the right of $\nu = x$. The two corresponding types of surface waves propagate in the fluid[2], with phase velocites close to that of a plane sound wave in the fluid, while the following surface waves propagate in the elastic cylinder, with phase velocites comparable to those of the elastic waves:

A single "Rayleigh (R) pole" ν_R with moderately large imaginary part (which tends towards the conventionally defined Rayleigh pole on a flat half-space[2,5] as $ka \to \infty$) lies near $\nu = x_T$, and a series of "Whispering Gallery (WG) poles" ν_{WG} with small imaginary parts trails towards the left from x_T and x_L. (Note that the poles in the second quadrant of the ν-plane do not contribute and are not enclosed in the contour C_1, since they would give rise to surface waves that increase exponentially with time). We have also located[6] a few "unclassified poles" near x_L and x_T, not shown in Fig. 2.

As ka increases, more poles move into the first quadrant from left, rendering the pole series more dense and resulting

in a larger number of propagating circumferential wave modes. In the limit of $ka \to \infty$ (e.g., flat half-space limit), the density of poles also tends to infinity, with the Whispering Gallery pole series tending towards the lateral waves obtained from a branch cut integral[9].

2) Surface Wave Resonances

We now show that the surface waves described by the scattering amplitudes of Eqs. (10b,c) contain Regge poles of the form of Eq. (3). The ℓ th zero of $D_\nu(\omega)$,

$$\nu_\ell(\omega) = Re\ \nu_\ell(\omega) + i\ Im\ \nu_\ell(\omega), \tag{14}$$

which is a function of the frequency, will at some "resonance frequency" $\omega = \omega_{n\ell}$ move past the integer n, so that Re ν $(\omega_{n\ell}) = n$. In the vicinity of the resonance frequency where $\nu_\ell = n + \delta\nu_\ell$, and assuming $Im\ \nu_\ell \ll 1$, one has

$$\frac{1}{\sin \pi \nu_\ell} \cong \frac{1}{(-1)^n \pi\, \delta\nu_\ell} = \frac{(-1)^n}{\pi} \frac{1}{\nu_\ell - n}. \tag{15}$$

If we now identify Re $\nu_\ell = n\omega$ and $Im\,\nu_\ell = \frac{1}{2}\hat{\Gamma}$, then Eq. (15) and hence the scattering amplitudes p_1, p_2 of Eqs. (10b, c) assume precisely the Regge pole form of Eq. (3). This shows that as the incident frequency ω passes through the nth resonance frequency of the ℓth surface wave $\omega_{n\ell}$, the corresponding surface wave goes through a resonance. This is illus-

trated[10] in Fig. 3, which shows on a logarithmic scale the contribution to $|p_1|$ of the Rayleigh wave ($\ell = R$) on an aluminum cylinder in water, for the case of back scattering ($\varphi = \pi$), plotted vs. $ka \equiv \omega a/c$. The narrow resonances which occur at the values of $ka = \omega_{nR} a/c$, and whose width is determined by $Im\ \nu_R$, are clearly visible.

It is not hard to explain the physical origin of these resonances with the help of Eq. (11). The latter shows that for $m = 0$, two surface waves propagate in the counterclockwise ($\lambda = 1$) and in the clockwise ($\lambda = -1$) direction around the cylinder, joined by other such waves with $m > 0$ that already have encircled the cylinder m times previously (of course with larger and larger attenuation since $Im\ \nu_\ell \neq 0$), due to the steady-state situation considered here. The wavelength is given by

$$\lambda_\ell = \frac{2\pi a}{Re\ \nu_\ell(\omega)} \quad , \tag{16}$$

and at the resonance frequency $\omega = \omega_{n\ell}$ where $Re\ \nu_\ell = n$, one sees that exactly n wavelengths of the surface wave fit the circumference of the target, and hence lead to a resonant reinforcement of the circumferential wave in the course of its repeated circumnavigations.

II. Modal Resonances and Resonant Excitation of Eigenvibrations.

We turn next to the resonances in the scattering amplitude of the type of Eq. (1), written as a function of frequency ω at a fixed (real integer) mode number n. As is clear from the introduction, these are really the same resonances as the Regge poles of Eq. (3), simply rewritten in a different variable. In fact, the resonance amplitude could be represented as a two-dimensional surface in a three-dimensional space, plotted over the two axes ω and n, and having on it a series of roughly parallel ripples whose ridges run at an angle to either axis. These ripples appear as a resonance in ω if the surface is sliced at n = const (Eq. 1), or as a resonance in n if the surface is sliced at ω = const (Eq. 3). These ω-resonances will be illustrated below for the example of acoustic-wave scattering from an elastic cylinder, and further on for other examples of acoustic and elastic-wave scattering. They will be treated mathematically by the Breit-Wigner theory[11] developed for the resonances in nuclear scattering.

1) Acoustic Scattering from an Elastic Cylinder

We shall write the scattered portion of Eq. (5a) as

$$p_{sc} = \frac{1}{2} \sum_{n=0}^{\infty} \varepsilon_n i^n \left(S_n - 1 \right) H_n^{(1)} (kr) \cos n\varphi \qquad (17)$$

where we introduced the scattering function $S_n \equiv \exp(2i\delta_n)$ of the nth mode, familiar from nuclear scattering theory with δ_n the scattering phase shift; here,

$$S_n = 1 + 2b_n / D_n . \tag{18}$$

For a rigid cylinder, one has, incidentally[12]:

$$S_n^{(0)} = 1 - 2 J_n'(ka) / H_n^{(1)\prime}(ka) . \tag{19}$$

Let us consider the far-field value of p_{sc} by employing the Hankel asymptotic form for $kr \gg n$,

$$H_n^{(1)}(kr) \sim (2/\pi i k r)^{1/2} i^{-n} e^{ikr} , \tag{20}$$

and introduce the far-field scattering "form function"

$$f(\varphi) = \sum_{n=0}^{\infty} f_n(\varphi), \tag{21}$$

consisting of "partial wave" contributions

$$f_n(\varphi) = (\pi i k a)^{-1/2} \varepsilon_n (S_n - 1) \cos n\varphi . \tag{22}$$

In terms of this, p_{sc} becomes asymptotically

$$p_{sc} \sim (a/2r)^{1/2} e^{ikr} f(\varphi) . \tag{23}$$

Following Reference 3, the expression for S_n may be represented as

$$S_n = S_n^{(0)} \frac{F_n^{-1} - Z_2^{-1}}{F_n^{-1} - Z_1^{-1}} , \tag{24a}$$

where, from Eq. (19),

$$S_n^{(0)} = -\frac{H_n^{(2)\prime}(x)}{H_n^{(1)\prime}(x)} \equiv e^{2i\xi_n} \tag{24b}$$

represents the S-function for scattering from a rigid cylinder. The corresponding phase shift is

$$\tan \xi_n = J_n'(x) / Y_n'(x). \tag{25}$$

We further used

$$z_i = x\, H_n^{(i)\prime} / H_n^{(i)}(x), \qquad i = 1, 2, \tag{26}$$

and defined the quantity

$$F_n(x) = \frac{\rho_w}{\rho_c} x_T^2 \frac{D_n^{(1)}}{D_n^{(2)}}, \tag{27}$$

a function of the normalized frequency x, with ρ_c, ρ_w the densities of the cylinder and of the ambient fluid, respectively. Further,

$$D_n^{(1)} = \begin{vmatrix} a_{22} & a_{23} \\ a_{32} & a_{33} \end{vmatrix}, \qquad D_n^{(2)} = \begin{vmatrix} a_{12} & a_{13} \\ a_{32} & a_{33} \end{vmatrix}, \tag{28a}$$

$$\begin{aligned} a_{12} &= (x_T^2 - 2n^2) J_n(x_L) + 2 x_L J_n'(x_L), \\ a_{22} &= x_L J_n'(x_L) \\ a_{32} &= 2n \left[J_n(x_L) - x_L J_n'(x_L) \right], \\ a_{13} &= 2n \left[J_n(x_T) - x_T J_n'(x_T) \right], \end{aligned} \tag{28b}$$

$$a_{23} = n J_n(x_T),$$

$$a_{33} = (x_T^2 - 2n^2) J_n(x_T) + 2x_T J_n'(x_T).$$

The quantities z_i^{-1} may be separated into real and imaginary parts:

$$z_{1,2}^{-1} = \Delta_n \pm i s_n. \tag{29}$$

We now employ[13] the linear approximation method of nuclear resonance theory, in which we define resonance frequencies $x_n^{(r)}$ by the condition

$$F_n^{-1}(x_n^{(r)}) = \Delta_n(x_n^{(r)}), \tag{30}$$

an eigenvalue equation with a multiplicity of solutions ($r = 1,2,3 \ldots$). We expand $F_n^{-1} - \Delta_n$, assumed to be slowly varying with frequency, in a Taylor series in x in the vicinity of any of these resonance frequencies:

$$F_n^{-1}(x) - \Delta_n(x) \cong \beta_n^{(r)} (x - x_n^{(r)}). \tag{31a}$$

We also introduce a "resonance width" $\Gamma_n^{(r)}$ by the definition

$$\Gamma_n^{(r)} = -2 s_n / \beta_n^{(r)} \qquad (>0). \tag{31b}$$

The S-function may be rewritten in the resonance form

$$S_n \equiv e^{2i\delta_n} = \sum_r S_n^{(0)} \frac{x - x_n^{(r)} - \frac{1}{2} i \Gamma_n^{(r)}}{x - x_n^{(r)} + \frac{1}{2} i \Gamma_n^{(r)}}. \tag{32}$$

Note that due to the reality of the quantities involved, one has the "unitarity relations"

$$|S_n| = |S_n^{(o)}| = 1, \tag{33}$$

expressing the fact that no energy is lost in the scattering process. Furthermore, S_n is seen to possess not only a resonance pole at the complex frequency

$$\chi = \chi_p^{(n)} = \chi_n^{(r)} - \tfrac{1}{2} i \Gamma_n, \tag{34a}$$

cf Eq. (1), but also resonance zero at

$$\chi = \chi_z^{(n)} = \chi_n^{(r)} + \tfrac{1}{2} i \Gamma_n, \tag{34b}$$

necessary in order to satisfy the unitarity condition.

The quantity $S_n - 1$ which appears in the scattering amplitude, Eq. (17), and which has the form

$$S_n - 1 = 2i e^{i\delta_n} \sin\delta_n$$

$$= 2i e^{2i\xi_n} \left[\frac{S_n}{F_n^{-1} - \Delta_n - i S_n} + e^{-i\xi_n} \sin\xi_n \right], \tag{35a}$$

may be represented by the resonance expression

$$\frac{S_n - 1}{2i} = e^{2i\xi_n} \left[\sum_r \frac{\frac{1}{2}\Gamma_n^{(r)}}{\chi_n^{(r)} - \chi - \frac{1}{2} i \Gamma_n^{(r)}} + e^{-i\xi_n} \sin\xi_n \right]. \tag{35b}$$

The partial-wave form function

$$f_n(\varphi) = 2i\varepsilon_n (\pi i ka)^{-1/2} e^{i\delta_n} \sin\delta_n \cos n\varphi \qquad (36a)$$

of Eq. (22) then becomes

$$f_n(\varphi) = 2i\varepsilon_n (\pi i ka)^{-1/2} e^{2i\xi}\left[\sum_r \frac{\frac{1}{2}\Gamma_n^{(r)}}{X_n^{(r)} - X - \frac{1}{2}i\Gamma_n^{(r)}} + e^{-i\xi_n}\sin\xi_n\right]\cos n\varphi \qquad (36b)$$

where the second term in the brackets represents a rigid-cylinder "potential scattering" background contribution, upon which a number of resonances ($\sum_r$) are superimposed, and with which they interfere.

This is illustrated in Fig. 4a where we plot $|f_n(\pi)|$ from Eqs. (22) and (24a) vs. $x \equiv ka$, for a number of partial waves n. In each amplitude, one recognizes a series of narrow resonance features superimposed on a smooth background, which is found to be given by the scattering amplitudes of the rigid cylinder. In fact, if we subtract the rigid-cylinder scattering amplitude $f_n^{(0)}(\pi)$ from $f_n(\pi)$ and plot the resulting quantity $|f_n(\pi) - f_n^{(0)}(\pi)|$ as shown in Fig. 4b, then essentially only the resonance contribution appears and the widths of the resonances can easily be determined.

The total form function $f(\varphi)$, which is the physically measured quantity, is given by Eq. (21). In Fig. 4c, we plot $|f(\pi)|$ vs. $x = ka$ and observe, comparing with Fig. 4a, that all the resonances appear here simultaneously, which

explains the extremely irregular appearance of the total form function.

The displacement field in the interior of the cylinder, $\vec{u}$, may be represented in terms of two potentials Ψ, A, in the form

$$\vec{u} = -\vec{\nabla}\Psi + \vec{\nabla} \times \vec{A} \,. \tag{37a}$$

If the corresponding solutions[2] are subjected to the resonance formalism[13], one find, e.g.,

$$\Psi = \frac{2}{\pi i \rho_w \omega^2} \sum_{n=0}^{\infty} \sum_{r} \frac{\varepsilon_n i^n}{\beta_n^{(r)}} \frac{a_{33}}{x H_n^{(1)\prime}(x) D_n^{(1)}} \frac{J_n(k_L r)\cos n\varphi}{x - x_n^{(r)} + \frac{1}{2} i \Gamma_n^{(r)}} \,, \tag{37b}$$

showing that the interior solution consists of pure resonances without any background term. Since the resonances are narrow, we find the important result that the external acoustic field penetrates the cylinder only at frequencies near one of the resonance frequencies, while little penetration into the interior occurs in between the resonances, in agreement with Section III.

When passing through a resonance, the phase of f_n is expected to jump through π over a frequency interval of the order Γ_n; in fact, from Eq. (32) one finds

$$\delta_n = \xi_n + \tan^{-1} \frac{\Gamma_n^{(r)}}{2(x_n^{(r)} - x)} \tag{38}$$

which confirms this conclusion. Fig. 5 shows the phase $\delta_n + \frac{1}{4}\pi$ plotted modulo 2π above $|f_n(\pi)|$ for n = 2. Here, the linear behavior stems from ξ_n, the superimposed jumps of 2π from the resonances.

Returning to Figs. 4, we may discern families of resonances labeled $\ell = 1,2,3...$ whose members appear in all the partial waves, shifting to higher frequencies from one partial wave to the next (hence $\omega' > 0$, cf. Eq. (2)). They may be identified with the elastic surface-wave Regge poles shown in Fig. 2, $\ell = 1$ representing the Rayleigh wave and $\ell = 2,3...$ the Whispering Gallery waves. The partial-wave resonance families are each a successive manifestation of one corresponding Regge pole as it moves along its trajectory $\nu = \nu_n(\omega)$ in the complex ν-plane when the frequency is being varied, appearing as a resonance in $|f_n|$ as $\mathrm{Re}\,\nu_n(\omega_{n\ell}) = n$.

The various, strikingly different shapes of the resonances in Fig. 4a are explained by their interference with the background. A pure resonance, e.g. $(n,\ell) = (2,3)$, appears if it nearly coincides with a null of the background. If it coincides with a maximum of the background, e.g. (1,3), (3,3) or (5,2), a total cancellation and thus a narrow hole occurs; in the general case, e.g. (1,2), (2,2), the interference produces a dip on one side and a peak on the other side of the resonance.

What, physically, causes the nth mode to resonate at its eigenfrequencies $\omega_{n\ell}$? To find out, let us study the pro-

perties of the nth individual normal mode in Eq. (5a) or Eq. (17). Each mode is a multipole, with n = 0 the "breathing mode" (where the pressure contours move radially in and out), n = 1 the dipole (contour motion is rigidly back and forth), n = 2 the quadrupole (contours oscillate between pro - and oblate ellipses), etc., see Fig. 6a. All these motions represent standing waves, which may be resolved into a pair of waves $\exp i(\pm n\varphi - \omega t)$ traveling in the opposite sense, with modal phase velocity $c_n(\omega) = a\omega/n$ (since n/a represents here the propagation constant), and it is clear that for the nth mode, exactly n wavelengths fit over the circumference of the body. This property may be taken as the physical characteristic of a normal mode.

The above-discussed eigenfrequencies $\omega = \omega_{n\ell}$ of the cylinder appear as a multiplicity $\ell = 1,2,\ldots$ of eigenfrequencies for each given mode n. This multiplicity represents the possibility of various radial deformations of the pressure contours in the fluid, belonging to one and the same azimuthal deformation (the latter characterizing the mode uniquely). For example, the radial deformations of the pressure contours for the breathing mode (n = 0) may occur uniformly radially outward ($\ell = 1$), or outward near the cylinder but inward further away, with one "node" in between ($\ell = 2$), etc.

Eq. (13) now gives the phase velocity $c_\ell(\omega)$ of the ℓth surface wave (or Regge pole). Comparing with $c_n(\omega)$,

we see that at the resonance frequency $\omega = \omega_{n\ell}$ where $\mathrm{Re}\,\nu_\ell = n$, these two phase velocities coincide. We may therefore state that a cylinder resonance (n, ℓ) occurs at that frequency where the phase velocity of the ℓ th surface wave coincides with the nth modal phase velocity, as sketched in Fig. 6b. The multiplicity of resonance frequencies for one given mode is hence explained naturally by the multiplicity of the existing surface waves.

2) Acoustic Scattering from an Elastic Sphere.

The theory of this case is exactly analogous to that of the cylinder, the essential difference being a replacement of cylindrical by spherical Bessel, Hankel, etc. functions. With an incident wave

$$p_{inc} \equiv e^{ikr\cos\vartheta} = \sum_{n=0}^{\infty} (2n+1)\, i^n j_n(kr)\, P_n(\cos\vartheta) \tag{39}$$

and a scattered wave

$$p_{sc} = \frac{1}{2} \sum_{n=0}^{\infty} (2n+1)\, i^n (S_n - 1)\, h_n^{(1)}(kr)\, P_n(\cos\vartheta), \tag{40}$$

one obtains an S-function

$$S_n \equiv e^{2i\delta_n} = S_n^{(0)}\, \frac{F_n^{-1} - Z_2^{-1}}{F_n^{-1} - Z_1^{-1}} \tag{41a}$$

where

$$S_n^{(0)} = -\frac{h_n^{(2)}(x)}{h_n^{(1)}(x)} \equiv e^{2i\xi_n} \tag{41b}$$

corresponds to the rigid sphere,

$$z_i = x\, h_n^{(i)\prime}(x) / h_n^{(4)}(x) \quad , \quad i = 1, 2, \tag{41c}$$

and F_n is given by Hickling[14]. The form function of the nth partial wave is found as

$$f_n(\vartheta) = (2/ka)(2n+1)\, e^{i\delta_n} \sin\delta_n\, P_n(\cos\vartheta) \tag{42a}$$

$$\cong \frac{2}{ka}(2n+1) e^{2i\xi_n}\left[\sum_r \frac{\frac{1}{2}\Gamma_n^{(r)}}{x_n^{(r)} - x - \frac{1}{2}i\Gamma_n^{(r)}} + e^{-i\xi_n}\sin\xi_n\right] P_n(\cos\vartheta) \tag{42b}$$

using the same resonance formalism as before. A number of partial waves $|f_n(\pi)|$ using Eq. (41a) is plotted in Fig. 7, showing the corresponding resonances interfering with the rigid background.

3) Acoustic Scattering from an Elastic Cylindrical Shell.

The theory of this case may here be taken over directly from that of the cylinder, with only the replacement of D_n and b_n by corresponding 6 x 6 determinants for the shell which are given in the literature[15]. We here plot[16] in Fig. 8 several partial-wave form functions $|f_n(\pi)|$ for an air-filled aluminum shell in water, for various b/a (inner to outer-radius) ratios. Besides a shift of the resonances as compared to Fig. 4a, we also note that between b/a = 0.90 and 0.975, the background changes over from that of a rigid cylinder to that of a soft

cylinder surrounded by a negligible amount of shell material.

4) Elastic Wave Scattering from a Cylindrical Cavity.

The elastic waves incident on a fluid-filled cavity in an elastic body of density ρ are again described by a scalar and a vector potential Ψ , $\vec{A}$ as in Eq. (37a). For a compressional wave incident on a cylindrical cavity,

$$\Psi_{inc} = \sum_{n=0}^{\infty} \varepsilon_n i^n J_n(k_L r) \cos n\vartheta \tag{43a}$$

one has the scattered waves

$$\Psi_{sc} = \sum_{n=0}^{\infty} \varepsilon_n i^n (a_n / D_n) H_n^{(1)}(k_L r) \cos n\vartheta, \tag{43b}$$

$$A_{z\,sc} = \sum_{n=0}^{\infty} \varepsilon_n i^n (b_n / D_n) H_n^{(1)}(k_T r) \sin n\vartheta, \tag{43c}$$

the latter corresponding to mode conversion into a scattered shear wave. In the interior fluid, one has

$$\Psi_F = \sum_{n=0}^{\infty} \varepsilon_n i^n (c_n / D_n) J_n(k_F r) \cos n\vartheta \tag{43d}$$

where $k_F = \omega / c_F$, c_F being the sound velocity in the fluid (of density ρ_F). The boundary conditions at the cylinder radius $r = a$ determine the coefficients a_n, b_n, c_n and D_n in the form of 3 x 3 determinants composed of cylinder functions [17].

Introducing two elements of the 2 x 2 scattering matrix S_n by

$$S_n^{PP} = 1 + 2a_n / D_n$$
$$S_n^{PS} = 2b_n / D_n \qquad (44)$$

and using the asymptotic forms of $H_n^{(1)}(k_{L,T}r)$, the asymptotic potentials are found as

$$\Psi_{sc} \sim r^{-1/2} e^{ik_L r} \sum_{n=0}^{\infty} f_n^{PP}(\vartheta),$$
$$A_{z\,sc} \sim r^{-1/2} e^{ik_T r} \sum_{n=0}^{\infty} f_n^{PS}(\vartheta), \qquad (45)$$

with partial-wave scattering amplitudes

$$f_n^{PP} = (2\pi i k_L)^{-1/2} \varepsilon_n (S_n^{PP} - 1) \cos n\vartheta,$$
$$f_n^{PS} = (2\pi i k_T)^{-1/2} \varepsilon_n S_n^{PS} \sin n\vartheta. \qquad (46)$$

A very similar analysis can be performed for the case of an incident shear wave[18], which yields corresponding matrix elements S_n^{SP}, S_n^{SS}, completing the 2 x 2 scattering matrix

$$S_n = \begin{pmatrix} S_n^{PP} & S_n^{PS} \\ S_n^{SP} & S_n^{SS} \end{pmatrix} . \qquad (47a)$$

Unlike the case of acoustic scattering where Eq. (33) applied, one no longer has $|S_n^{PP}| = 1$ etc., but energy conservation only requires the overall scattering matrix S_n to be unitary,

$$S_n^{+} S_n = S_n S_n^{+} = 1, \qquad (47b)$$

due to the existence of mode conversion in the present case.

If we define the quantities

$$F_n(x_L) = \frac{\rho}{\rho_F} \frac{x_F J_n'(x_F)}{J_n(x_F)} , \tag{48a}$$

$$z_1 = -\tfrac{1}{2} x_T^2 \left(D_{11} D_{32} - D_{12} D_{31} \right) / \left(D_{21} D_{32} - D_{22} D_{31} \right)$$

$$= \Delta_n + i S_n \tag{48b}$$

where D_{ij} are the elements of D_n, and further similar quantities z_2 and $\tilde{z}_2$, as well as the empty-cavity limits ($\rho_F \to 0$) of the S matrix elements

$$S_n^{(0)\,PP} = e^{2i\xi_n}$$
$$S_n^{(0)\,PS} = e^{2i\tilde{\xi}_n} \tag{49}$$

etc., (with ξ_n, $\tilde{\xi}_n$ complex due to Eq. (47b)), we obtain

$$S_n^{PP} = e^{2i\xi_n} \left(z_2 - F_n \right) / \left(z_1 - F_n \right), \tag{50a}$$

$$S_n^{PP} - 1 = e^{2i\xi_n} \left[\left(z_2 - z_1 \right) / \left(z_1 - F_n \right) + 2i e^{-i\xi_n} \sin \xi_n \right], \tag{50b}$$

$$S_n^{PS} = e^{2i\tilde{\xi}_n} \left[\left(\tilde{z}_2 - z_1 \right) / \left(z_1 - F_n \right) + 1 \right]. \tag{50c}$$

The resonance theory now defines again the multiplicity

of resonance frequencies $x_L^{(ns)}$ for the nth partial wave (labeled s = 1, 2, 3 ...) as the multiple solutions of the eigenvalue equation

$$F_n(x_L^{(ns)}) = \Delta_n(x_L^{(ns)}) \tag{51a}$$

(corresponding to the eigenfrequencies of the fluid-filled cavity), and expands $F_n(x_L) - \Delta_n$ around these:

$$F_n(x_L) - \Delta_n(x_L) \cong \beta_n^{(s)} (x_L - x_L^{(ns)}). \tag{51b}$$

With a definition of the widths

$$\Gamma_n^{(s)} = -2\delta_n / \beta_n^{(s)} \tag{52}$$

and of the further quantities

$$M_n^{(s)} = (z_1 - z_2) / \beta_n^{(s)} \tag{53a}$$

$$\tilde{M}_n^{(s)} = (z_1 - \tilde{z}_2) / \beta_n^{(s)}, \tag{53b}$$

the resonance expressions for the S-matrix elements

$$S_n^{PP} - 1 = e^{2i\xi_n} \left[\sum_{s=1}^{\infty} \frac{M_n^{(s)}}{x_L - x_L^{(ns)} + \frac{i}{2}\Gamma_n^{(s)}} + 2ie^{-i\xi_n} \sin\xi_n \right], \tag{54a}$$

$$S_n^{PS} = e^{2i\tilde{\xi}_n} \left[\sum_{s=1}^{\infty} \frac{\tilde{M}_n^{(s)}}{x_L - x_L^{(ns)} + \frac{i}{2}\Gamma_n^{(s)}} + 1 \right] \tag{54b}$$

are obtained. We then recognize $f_n^{PP,SS}(\vartheta)$ as consisting of background terms corresponding to the empty-cavity scattering amplitudes, with a series of superimposed resonance amplitudes which will interfere with the background. Little penetration of the field into the cavity will occur for frequencies in between the resonance frequencies.

For the example of a water-filled cylindrical cavity in an aluminum body, using Eqs. (50), we have plotted the quantities $a^{-1/2}|f_n^{PP}(\pi)|$ and $a^{-1/2}|f_n^{PS}(\vartheta)/\sin n\vartheta|$ vs. x_L for the partial waves n = 0 through 4, as shown in Figs. 9a and 9b, respectively. These figures show the empty-cavity background with superimposed (interfering) narrow resonances, which correspond to the excitation of the eigenvibrations of the fluid within the elastic walls (they disappear if one lets $\rho_F \to 0$). The eigenfrequencies of the fluid, i.e., the roots of $D_n(x_L) = 0$, are given in the literature[19], and their real parts agree exactly with the resonance positions in our figures (which, naturally, are the same for f_n^{PP} and f_n^{Ps}).

Reference 19 also lists a different set of eigenfrequencies of the cavity which corresponds to vibrations of the walls, rather than of the interior fluid. These do not appear as resonances in Fig. 9, hence are believed to be only weakly excited in our scattering problem. Their excitation does take place, however, as shown for the pulse problem of the spherical cavity by Norwood and Miklowitz[20], where excitations of Rayleigh

and Franz waves in the cavity walls have been identified. This refers to the evacuated cavity, where wall motions are the only modes of vibration. (The corresponding wall resonances form part of our soft background amplitude.) Similar studies for the evacuated cylindrical cavity have been performed by Miklowitz and Peck[21].

For each partial wave n, the resonances are labeled by s = 1, 2, 3 ... ("fundamental" s = 1, and "overtones" s = 2, 3 ...). Fig. 9 shows that for a given type of vibration s, the corresponding resonance shifts to successively higher frequency values as one progresses upwards through successive partial waves. (The background shifts similarly but even more rapidly). As before, the sth resonances throughout all the partial waves are caused by a single (the sth) Regge pole in the scattering amplitude, corresponding to the sth zero of the denominator $D_n(x_L)$ with n treated as a continuous complex variable, and with x_L a real frequency. In Fig. 9, the trajectory of each Regge pole may be followed succesively through the progression of partial waves, where the pole becomes physically manifest at the integer values of n.

Elastic Wave Scattering from a Spherical Cavity

An investigation similar to the one described above is in progress for the case of a fluid-filled spherical cavity (G.C. Gaunaurd and H. Überall, J. Acoust. Soc. Amer., to be published); it also takes into account absorption in the external medium. This is treated by making the propagation constants of

the medium complex,

$$k_{L,S} \rightarrow k_{L,S}\,(1 + i\,\beta_{L,S}), \tag{55a}$$

and writing

$$\beta_L = (F + 2F_1)/(2\rho c_L^2),$$
$$\beta_S = F_1 / (2\rho c_S^2), \tag{55b}$$

as suggested by the Kelvin-Voigt model of viscoelasticity in the limit of weak absorption.

Figs. 10 show preliminary results of this investigation. Fig. 10a presents the moduli of the n=0 and n=1 spherical partial wave amplitudes $|f_n^{PP}|$ for a water-filled spherical cavity in non-absorptive aluminum (first row), the soft background amplitude moduli (second row), and the water resonance moduli obtained by subtracting the background from each partial wave amplitude (third row). Fig. 10b shows the corresponding results for the mode-converted f^{PS} amplitudes. Finally, Fig. 10c presents $|f_n^{PP}|$ with n=0 and 1 for an air-filled spherical cavity in rubber. The first row of the figure refers to non-absorptive rubber ($F=F_1=0$), the second ($F=F_1=10^7$ dyn/cm^2) and third row ($F=F_1=10^9$ dyn/cm^2) to absorptive rubber. The following observations can be made:

(a) Apart from the well-known giant monopole (n=0) resonance of the (evacuated or air-filled) spherical cavity in rubber, all resonances are exceedingly narrow. In fact, only the n=1 non-absorptive resonances, obtained with 10 times finer numerical resolution than the other parts of the figure, appear accurately

in Fig. 10c.

(b) Absorption seems to mainly affect the background amplitude only, which is logical since the latter refers to the evacuated cavity, thus stems from the (absorptive) walls exclusively. The effect of absorption consists in a filling-in of the zeros of the background of amplitude.

III. Conclusion

A study has been performed of the resonances excited in an elastic body by incident acoustic waves, and in a fluid-filled cavity by incident elastic waves. The resonances are caused by Regge poles in the scattering amplitude, and they may be studied either as a function of frequency ω for a given mode number n (partial wave or modal resonances), or as a function of mode number (in the complex $n \to \nu$ plane) for a given frequency ω. In the latter case, the resonances have been investigated by means of the Sommerfeld-Watson transformation, and in the former case, by means of the Breit-Wigner resonance theory of nuclear scattering. Application of this theory to the present topics serves to indicate the basic similarity between scattering problems in various branches of Physics, which may be further illustrated by a recent interpretation[22] of the nuclear giant multipole resonances in terms of Regge poles using the methods of the Introduction.

The scattering resonances have been identified with the eigenvibrations of the scatterer, and physical arguments have been presented for the causes of the resonant excitations of these eigenvibrations: i.e., a resonant reinforcement in the repeated circumnavigations of surface waves. We also found that in between the resonance frequencies, the scattering object appears impenetrable and provides the corresponding non-resonant background of an impenetrable body to the scattering amplitude.

References

1. See, e.g., R.G. Newton, The Complex j-Plane, W.A. Benjamin, Inc., New York, 1964
2. R.D. Doolittle, H. Überall, and P. Uginčius, J. Acoust. Soc. Amer. 43, 1 (1968); see also H. Überall "Surface Waves in Acoustics", in Physical Acoustics, vol. 10 (Academic, N.Y. 1973)
3. D. Brill and H. Überall, J. Acoust. Soc. Amer. 50, 921 (1971)
4. W. Franz, Z. Naturforschung A9, 705 (1954).
5. G.V. Frisk, J.W. Dickey, and H. Überall, J. Acoust. Soc. Amer. 58, 996 (1975)
6. J.W. Dickey, G.V. Frisk, and H. Überall, J. Acoust. Soc. Amer. 59, 1339 (1976).
7. H. Überall and H. Huang, "Acoustical Response of Submerged Elastic Structures Obtained Through Integral Transforms", in Physical Acoustics, W.P. Mason and R.N. Thurston, Eds. (Academic, New York, 1976), Vol. 12
8. J.W. Dickey and H. Überall, J. Acoust. Soc. Amer. (to be published)
9. G.V. Frisk and H. Überall, J. Acoust. Soc. Amer. 59, 46 (1976)
10. J.W. Dickey, Ph.D. thesis, Catholic University of America, Washington, D.C., 1977; J.W. Dickey and H. Überall, J. Acoust. Soc. Amer. (to be published)
11. E.P. Wigner, Phys. Rev. 70, 15 (1946); G. Breit and E.P. Wigner, Phys. Rev. 49, 519 (1936); H. Feshbach, D.C. Peaslee, and V.F. Weisskopf, Phys. Rev. 71, 145 (1947)

12. H. Überall, R.D. Doolittle, and J.V. McNicholas, J. Acoust. Soc. Amer. 39, 564 (1966)

13. L. Flax, L.R. Dragonette, and H. Überall, J. Acoust. Soc. Amer. (to be published). Note that a connection between resonances in the scattering amplitude and the eigenvibrations of the scatterer has been observed earlier: J.J. Faran, J. Acoust. Soc. Amer. 23, 405 (1951); R.H. Vogt and W.G. Neubauer, J. Acoust. Soc. Amer. 60, 15 (1976); H. Überall, L.R. Dragonette, and L. Flax, J. Acoust. Soc. Amer. 61, 711 (1977)

14. R. Hickling, J. Acoust. Soc. Amer. 34, 1582 (1962)

15. R.D. Doolittle and H. Überall, J. Acoust. Soc. Amer. 39, 272 (1966)

16. J.D. Murphy, E.D. Breitenbach, and H. Überall, J. Acoust. Soc. Amer. (to be published)

17. A.J. Haug, S.G. Solomon, and H. Überall, submitted to J. Sound Vib.

18. A.J. Haug, S.G. Solomon, and H. Überall, J. Acoust. Soc. Amer. (to be published)

19. Y.H. Pao and C.C. Mow, J. Acoust. Soc. Amer. 59, 1046 (1976)

20. F.R. Norwood and J. Miklowitz, J. Appl. Mech. 34, 735 (1967)

21. J. Miklowitz, Proc. Eleventh Int. Congr. Appl. Mech., Munich, Germany, 1964 (Springer Verlag, 1966), p. 469; J. C. Peck and J. Miklowitz, Int. J. Solids Structures 5, 437 (1969).

22. Ameenah R. Farhan, J. George, and H. Überall, to be published

Figure Captions

Fig. 1 Contours in the complex ν -plane used for the Watson Transformation

Fig. 2 Schematic positions of Regge poles for an aluminum cylinder in water, and splitting of contours. Pole positions labeled ν_R (Rayleigh pole), ν_S (Stoneley), ν_F (Franz), ν_{WG} (Whispering Gallery poles), and saddlepoint ν_s.

Fig. 3 Pressure amplitude radiated by the Rayleigh wave on an aluminum cylinder in water towards an observer, located in the backward direction ($\varphi = \pi$) at a distance r = 10a, plotted vs. ka.

Fig. 4 (a) Partial wave backscattering amplitude moduli $|f_n(\pi)|$ for an aluminum cylinder in water, plotted vs. ka for the first six partial waves (n = 0 to 5). Positions of the eigenfrequencies are labeled by (ℓ) in each partial wave

(b) Modulus of n =2 partial wave backscattering amplitude with rigid background subtracted, $|f_2(\pi) - f_2^{rig}(\pi)|$, for aluminum cylinder in water

(c) Total backscattering amplitude modulus, $|f(\pi)|$, for aluminum cylinder in water. Resonances are labeled by (n, ℓ).

Fig. 5 Phase $\mod 2\pi$ (top) and modulus (bottom) of n=2 partial-wave scattering amplitude for an aluminum cylinder in water

Fig. 6 (a) Pressure contours for multipoles n=0 through 3

(b) Travelling-wave pair of nth (here sketched as 2nd) normal mode, and surface waves ℓ.

Fig. 7 Same as Fig. 4(a), for an aluminum sphere in water

Fig. 8 (a) Moduli of n=0 and 1 partial-wave scattering amplitudes for an air-filled cylindrical aluminum shell in water, for inner-to-outer radius ratio b/a = 0.900. Rigid background is shown as a dashed line.

(b) Same as (a) for b/a = 0.975, with rigid (dashed) and soft (dotted) amplitude indicated

(c) Same as (a) for b/a = 0.995. Soft background is shown as a dotted line

(d) Modulus of nth partial wave (n=0,1,2) scattering amplitude for air-filled cylindrical aluminum shell in water with rigid background subtracted, for b/a = 0.600

(e) Same as (d) with soft background subtracted, for b/a = 0.995. Note the giant n=0 ("bubble") resonance at very low ka.

Fig. 9 (a) Modulus of normalized backscattering amplitude $a^{-1/2}|f_n^{PP}(\pi)|$ vs. x_L, of compressional wave incident on water-filled cylindrical cavity in aluminum, for partial waves n=0 through 4. Reso-

nances at the fundamental eigenfrequencies of the water content of the cavity are labeled by $s = 1$, and at the overtones by $s = 2, 3, \ldots$

(b) Same as (a), for the mode-converted scattering amplitude $a^{-1/2}|f_n^{PS}(\vartheta)/\sin n\vartheta|$.

Fig. 10 (a) Modulus of backscattering amplitude $|f_n^{PP}|$ vs. x_L, of compressional wave incident on water-filled spherical cavity in aluminum, for partial-waves $n = 0$ and 1(first row); corresponding soft background (second row), and modulus of total amplitude (third row) less background.

(b) Same as Fig. 10(a), for $|f_n^{PS}|$

(c) $|f_n^{PP}|$ vs. x_L, for compressional wave incident on air-filled spherical cavity in rubber, for partial waves $n = 0$ and 1, with no absorption (first row), and absorption levels $F=F_1=10^7$ dyn/cm^2 and 10^9 dyn/cm^2 (second and third row, respectively).

Fig. 1

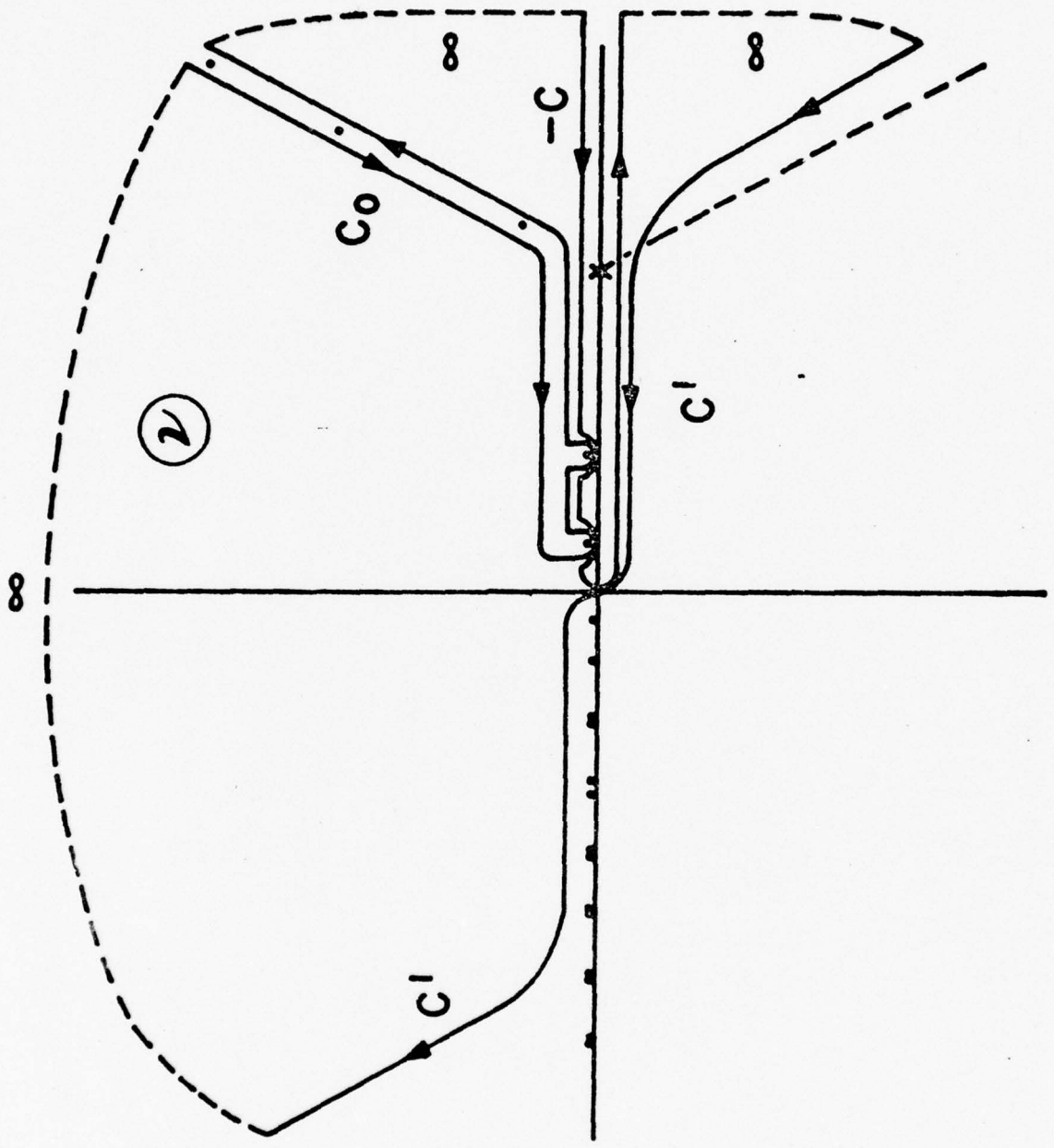

Fig. 2

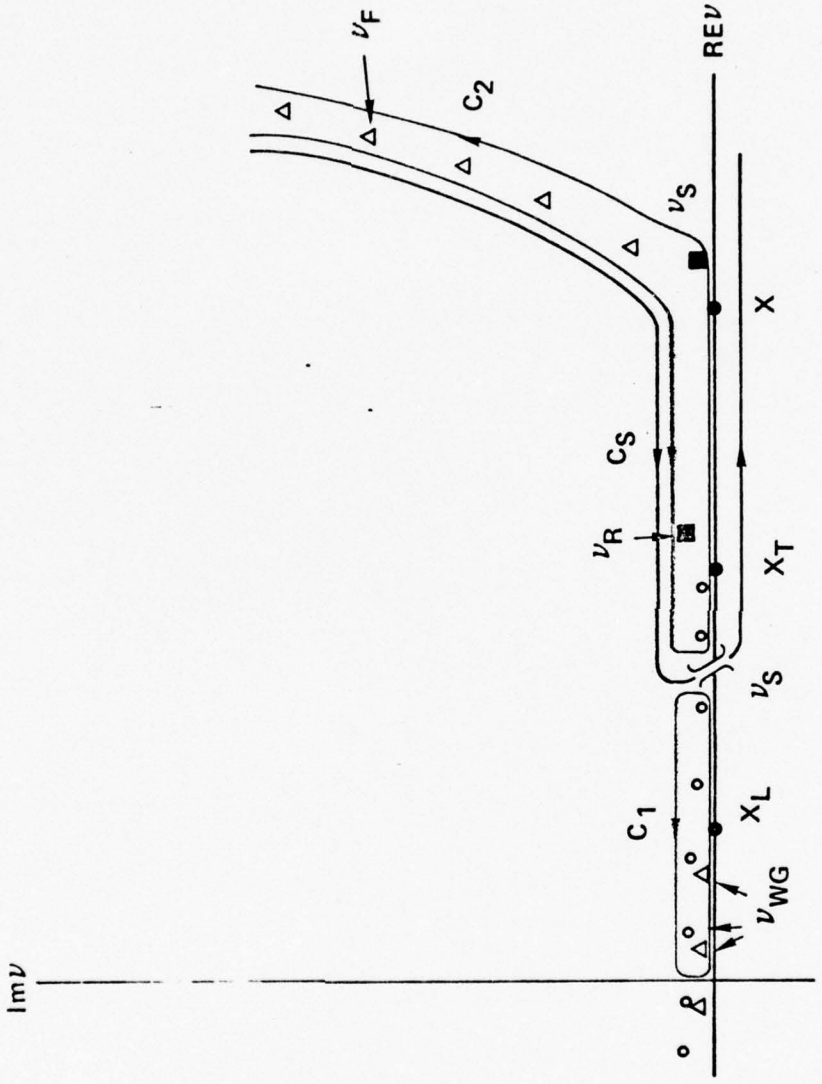

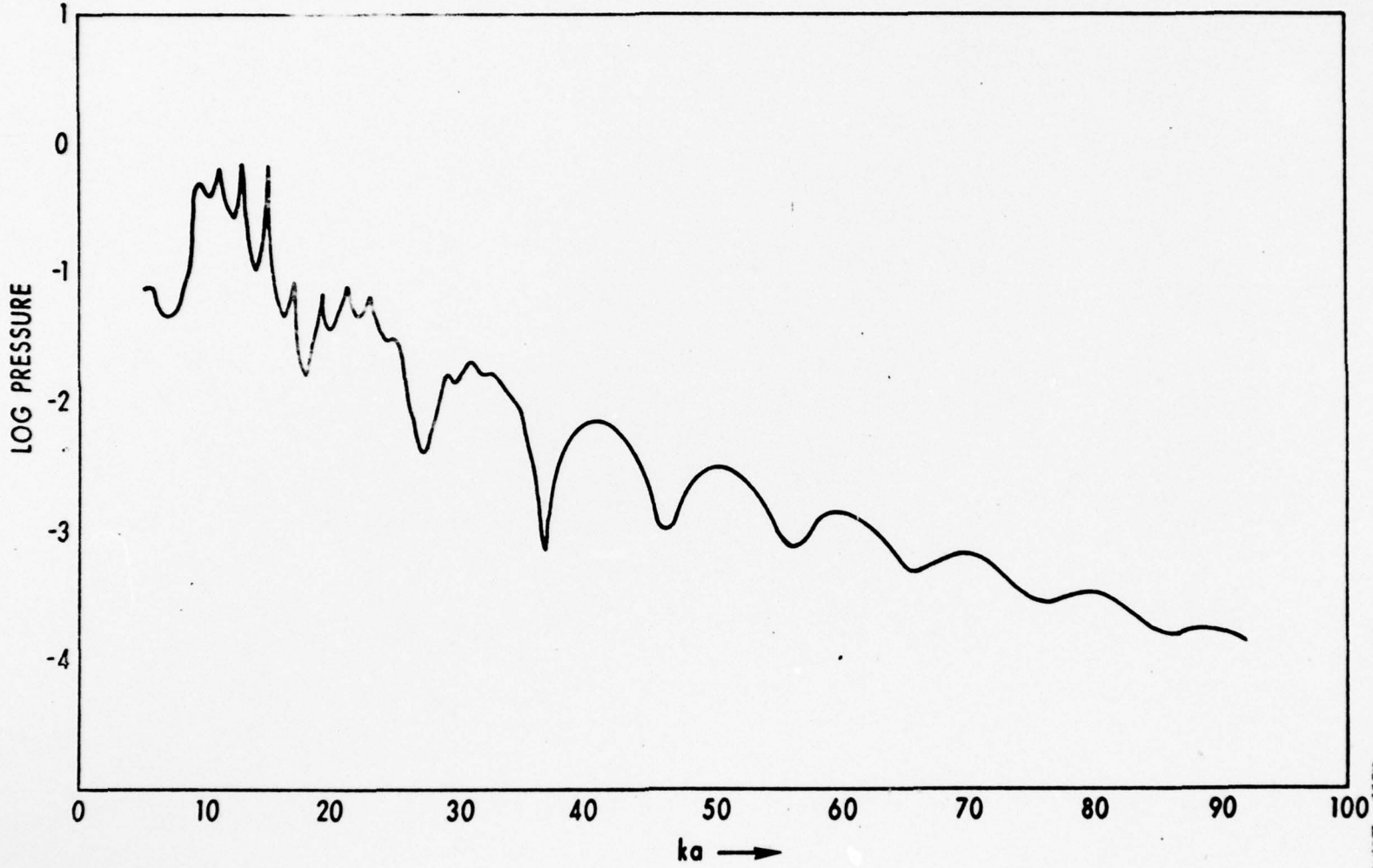

Fig. 3

Fig. 4a

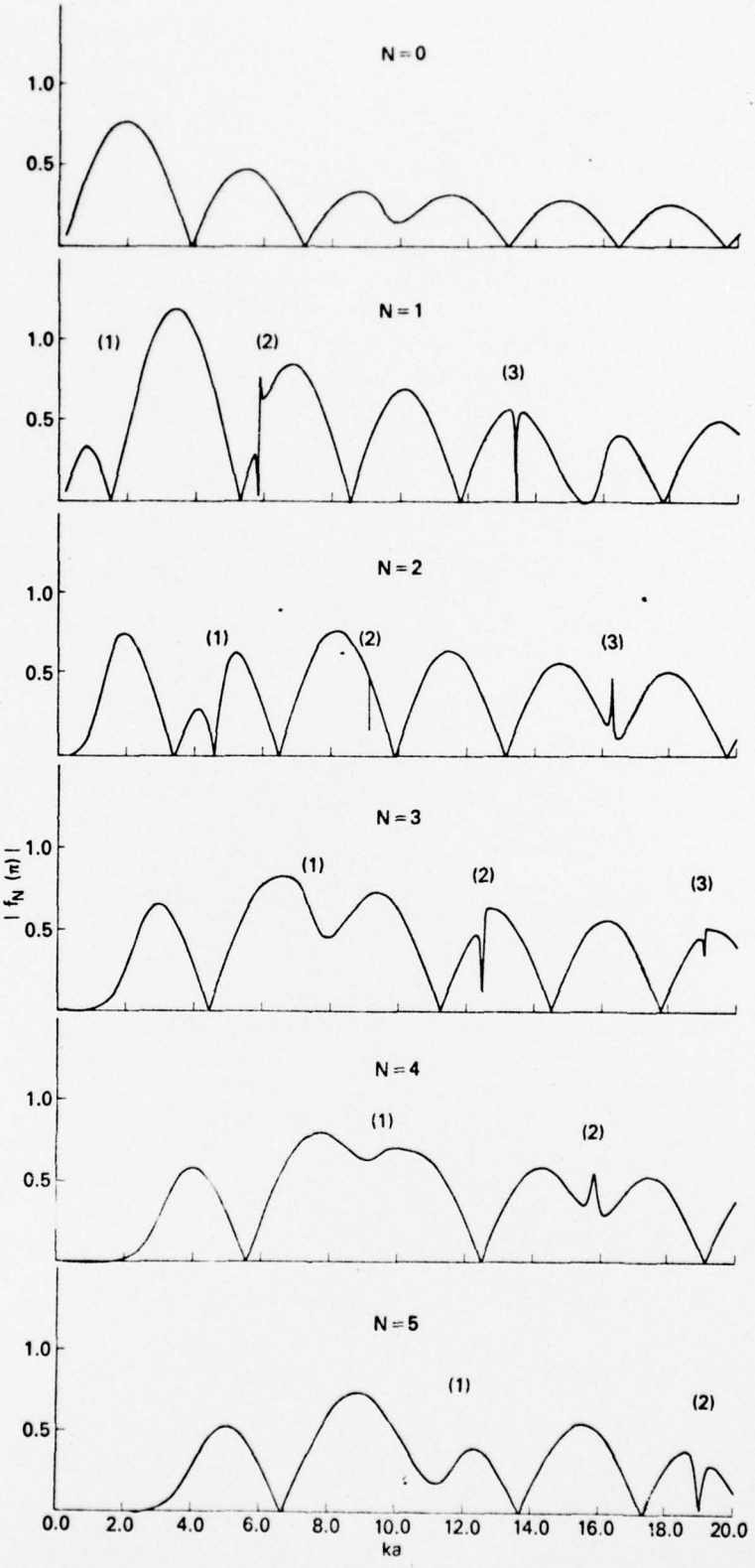
N = 0
N = 1
N = 2
N = 3
N = 4
N = 5
(1)
(2)
(3)
1.0
0.5
$|f_N(\pi)|$
0.0
2.0
4.0
6.0
8.0
10.0
12.0
14.0
16.0
18.0
20.0
ka

Fig. 4 b

| f2 (π)−f2RIGID (π) |
1.5
1.2
0.9
0.6
0.3
0.0
2.0
4.0
6.0
8.0
10.0
12.0
14.0
16.0
18.0
20.0
ka

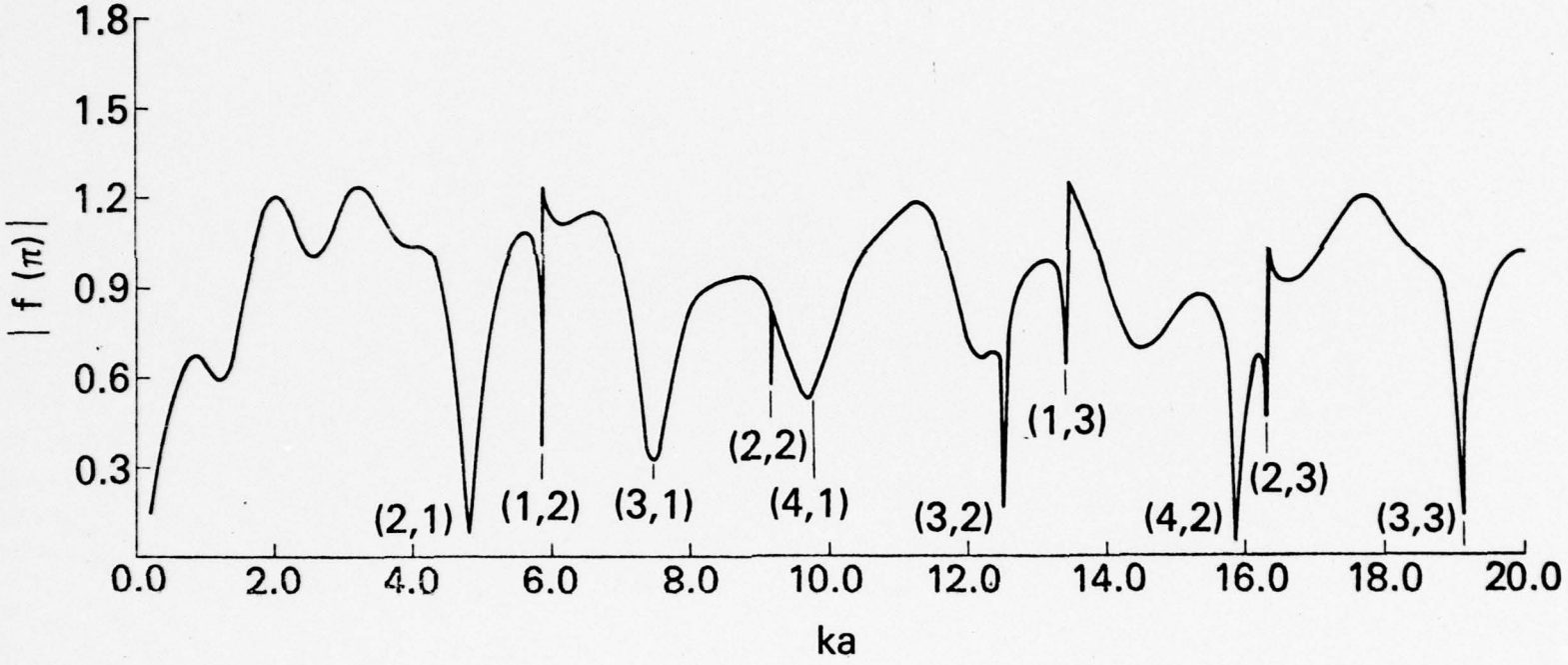
1.8
1.5
1.2
0.9
0.6
0.3
| f (π) |
(2,1)
(1,2)
(3,1)
(2,2)
(4,1)
(3,2)
(1,3)
(4,2)
(2,3)
(3,3)
0.0
2.0
4.0
6.0
8.0
10.0
12.0
14.0
16.0
18.0
20.0
ka

Fig. 4c

Fig. 5

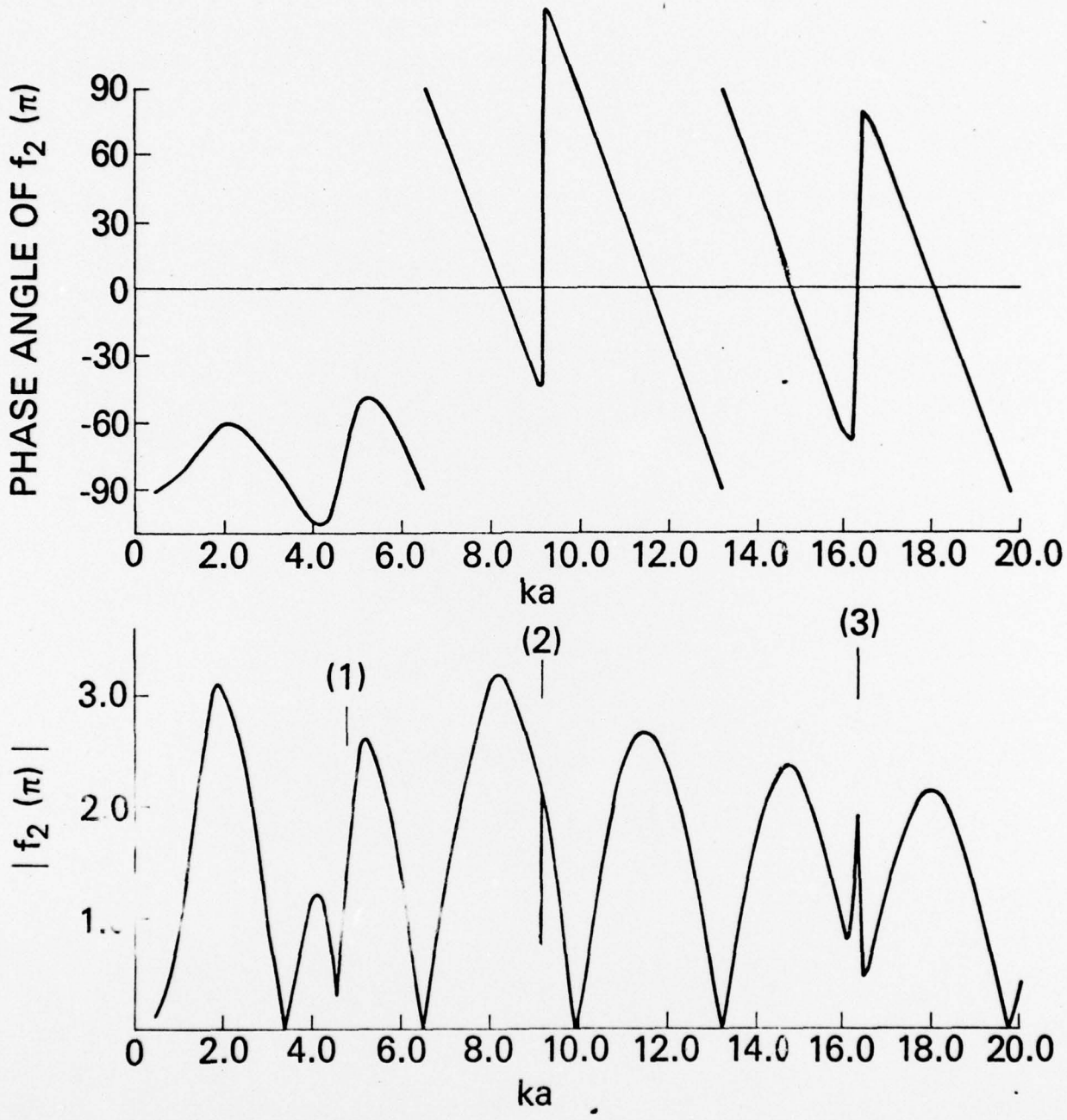
PHASE ANGLE OF f_2 (π)
90
60
30
0
-30
-60
-90
0
2.0
4.0
6.0
8.0
10.0
12.0
14.0
16.0
18.0
20.0
ka
$|f_2(\pi)|$
3.0
2.0
1.
(1)
(2)
(3)
0
2.0
4.0
6.0
8.0
10.0
12.0
14.0
16.0
18.0
20.0
ka

Fig. 6a

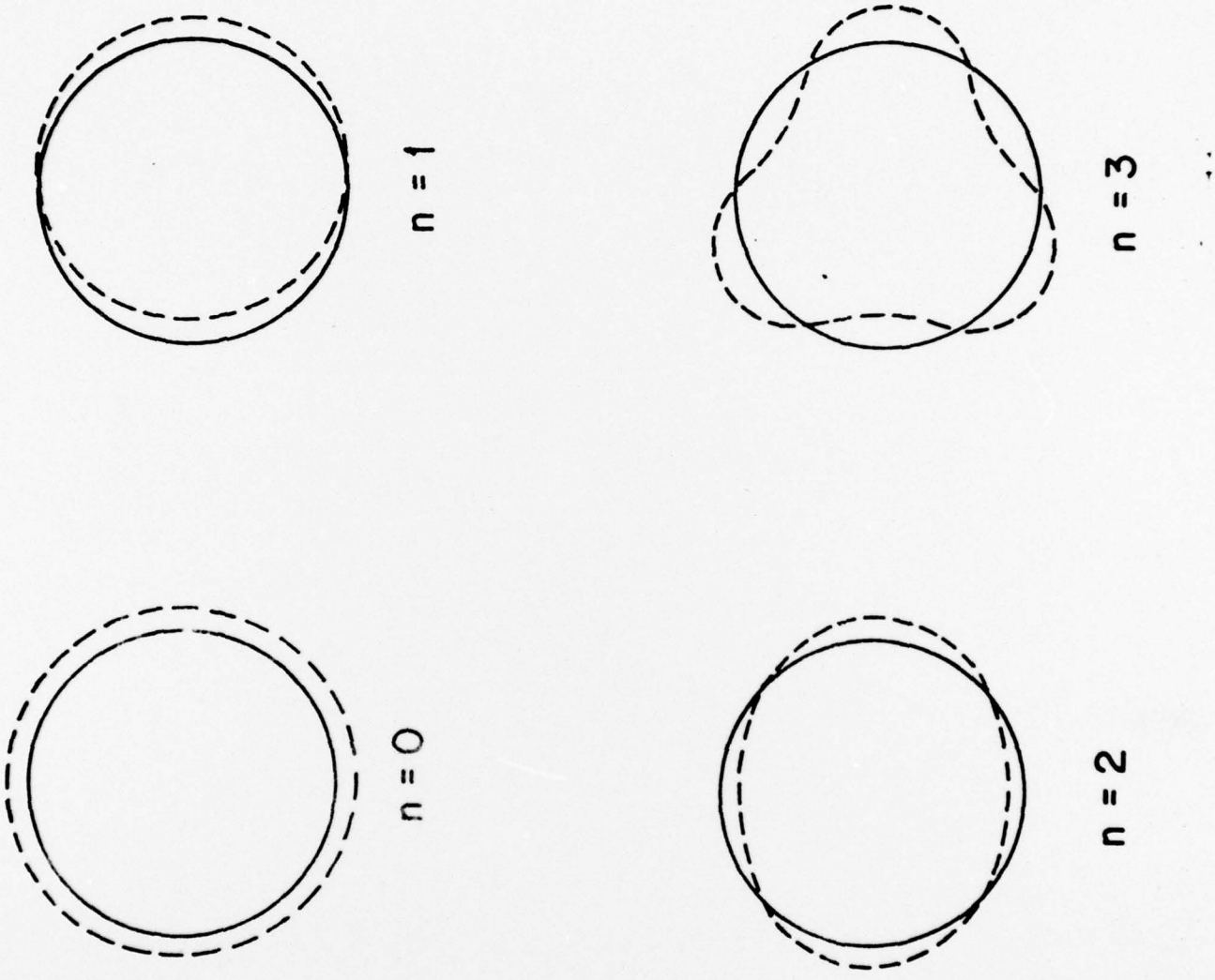

Fig. 6b

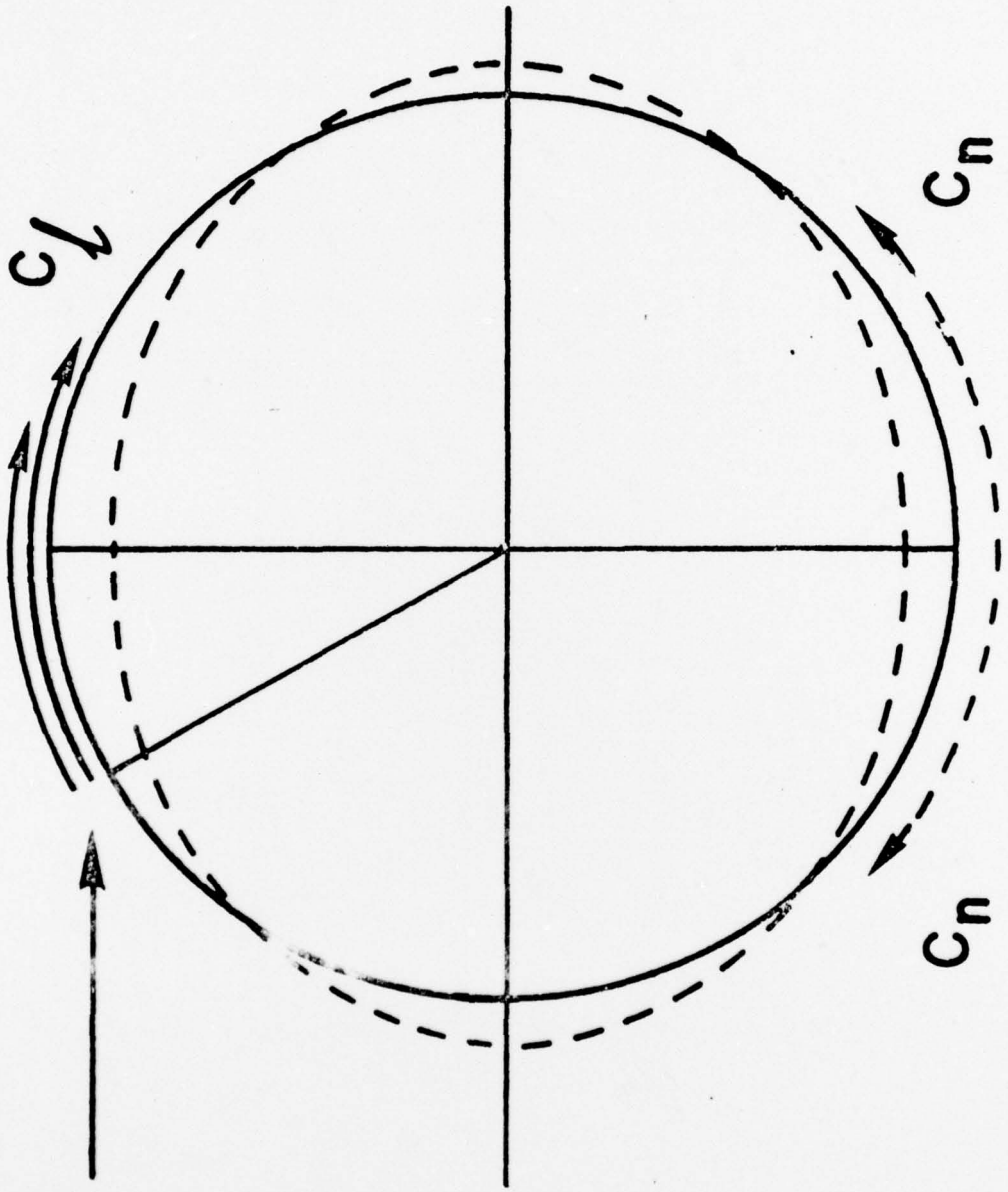

Fig. 7

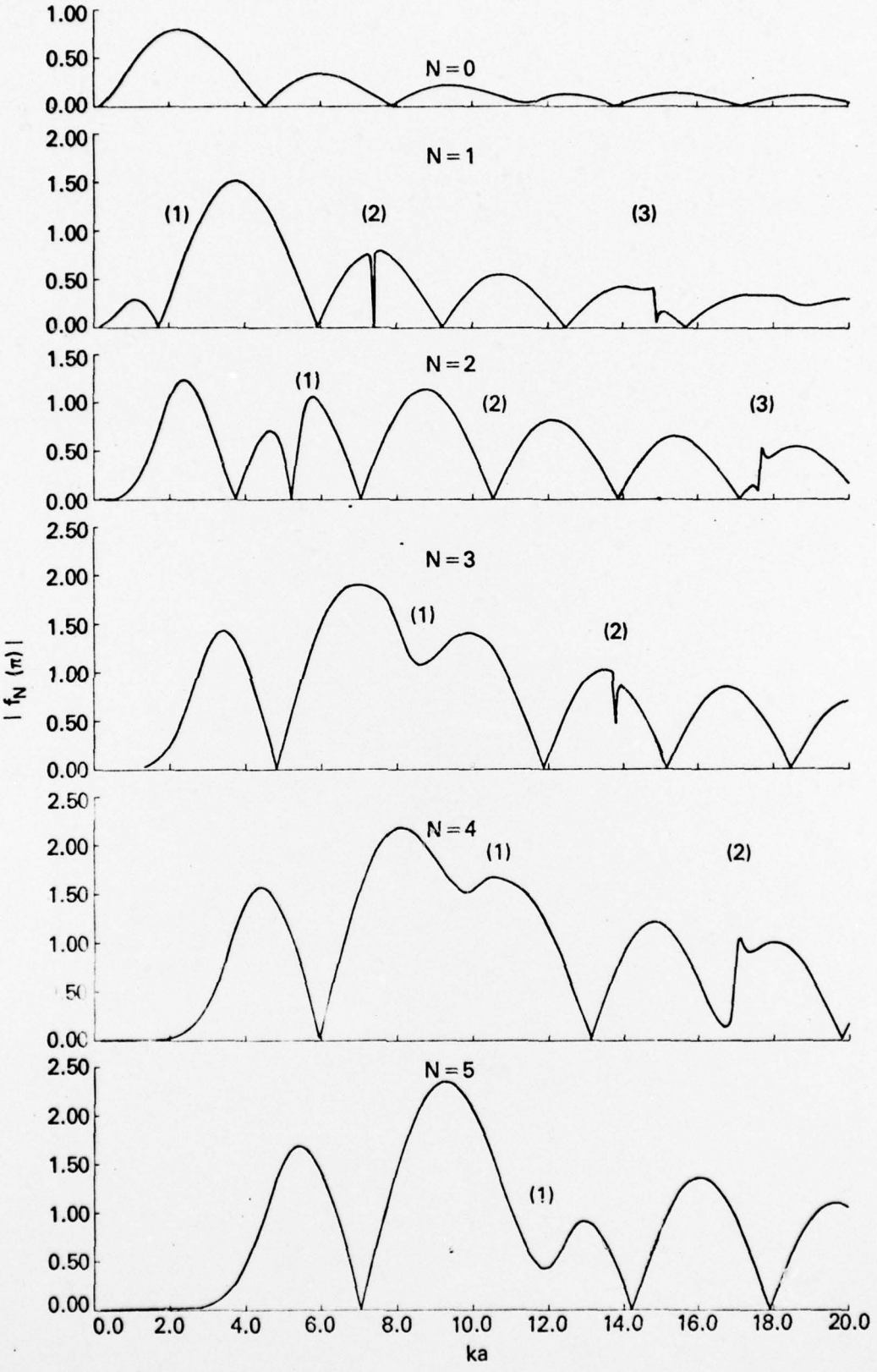
N = 0
N = 1
(1)
(2)
(3)
N = 2
(1)
(2)
(3)
N = 3
(1)
(2)
N = 4
(1)
(2)
N = 5
(1)
| f_N (π) |
ka
0.0
2.0
4.0
6.0
8.0
10.0
12.0
14.0
16.0
18.0
20.0

Fig. 8

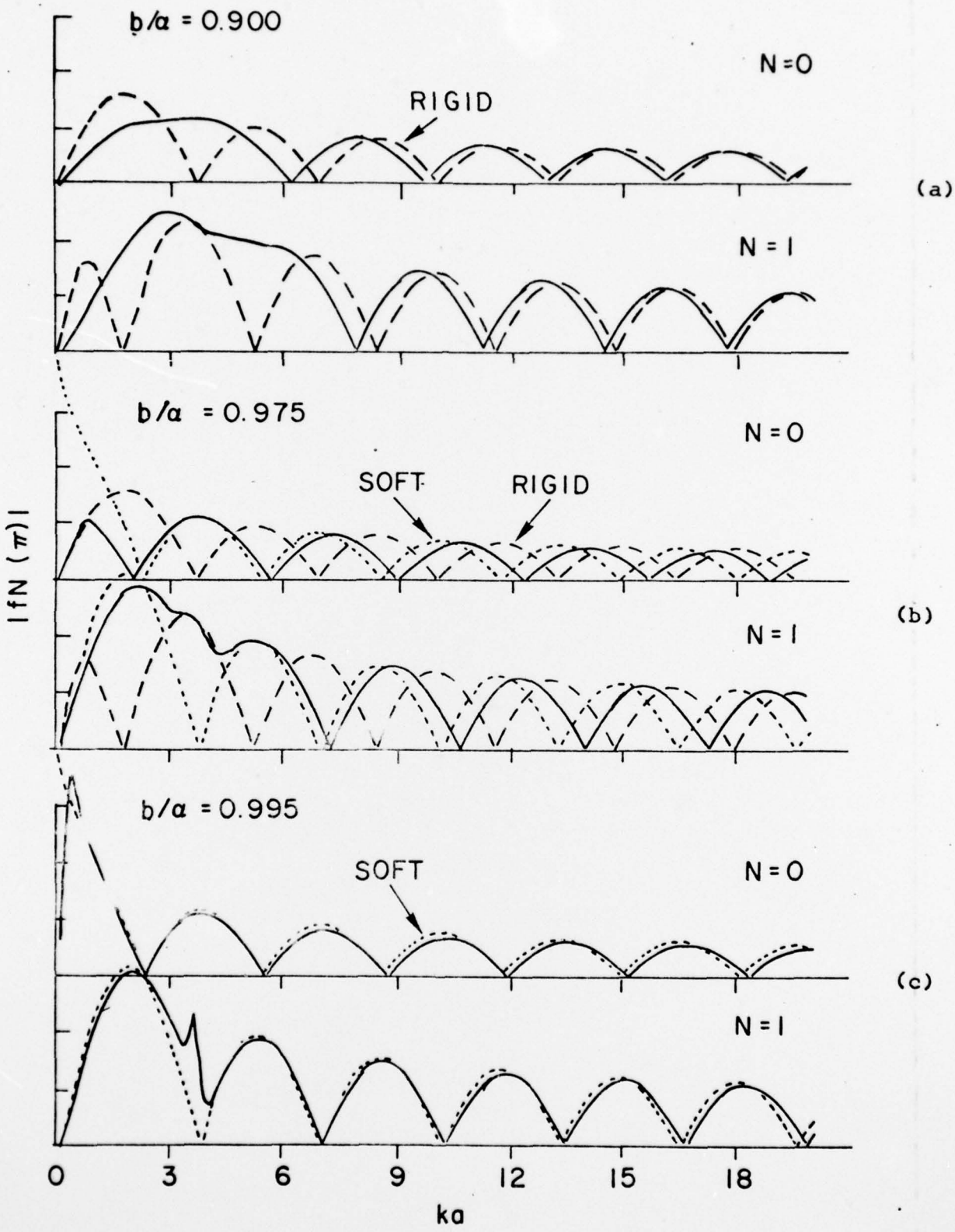
b/a = 0.900
N=0
RIGID
(a)
N = 1
b/a = 0.975
N=0
SOFT
RIGID
|fN (π)|
(b)
N = 1
b/a = 0.995
SOFT
N=0
(c)
N = 1
0
3
6
9
12
15
18
ka

Fig. 8

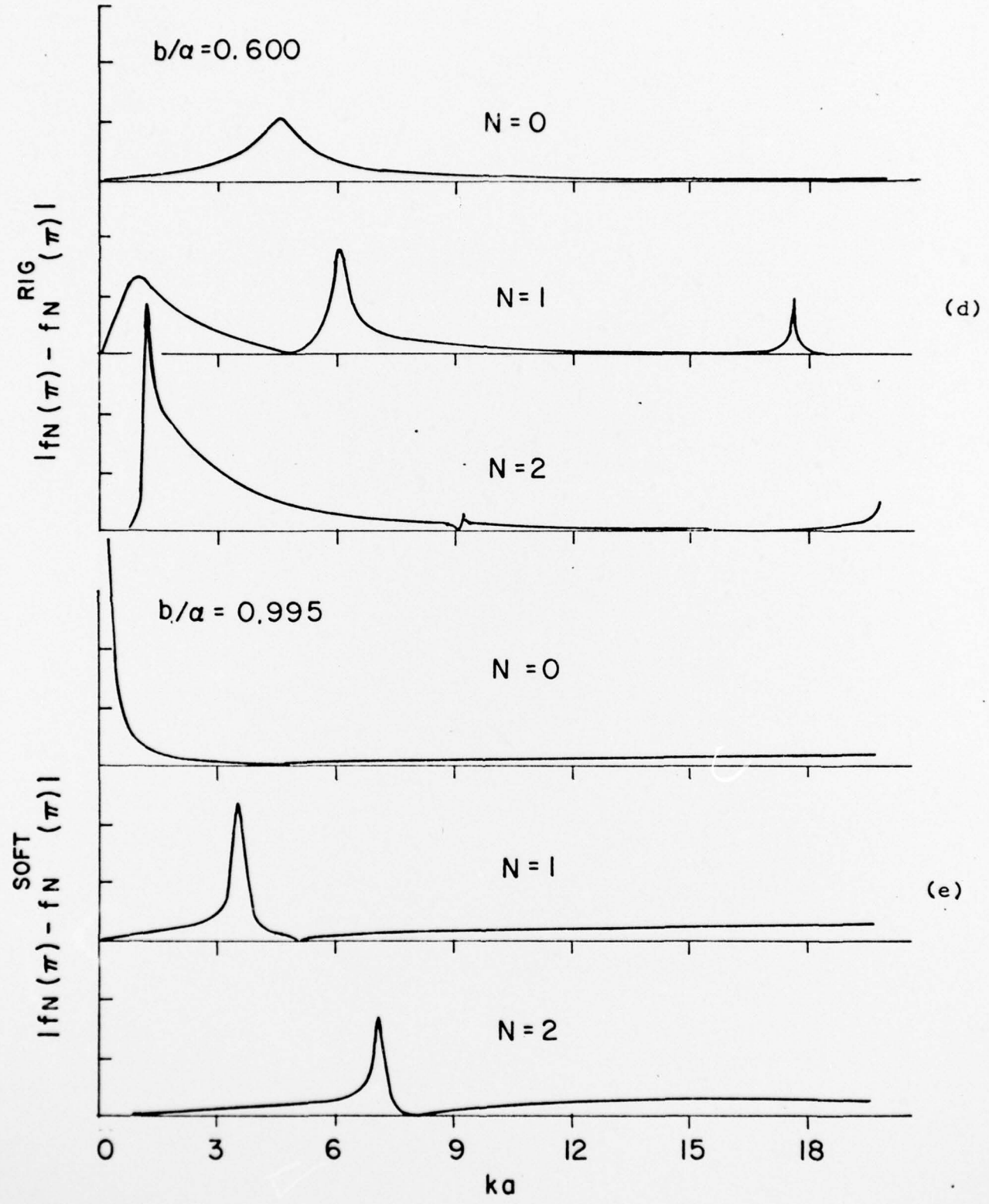
b/a =0.600
N = 0
N = 1
N = 2
$|f_N(\pi) - f_N^{RIG}(\pi)|$
(d)
b/a = 0.995
N = 0
N = 1
N = 2
$|f_N(\pi) - f_N^{SOFT}(\pi)|$
(e)
0
3
6
9
12
15
18
ka

Fig. 9a

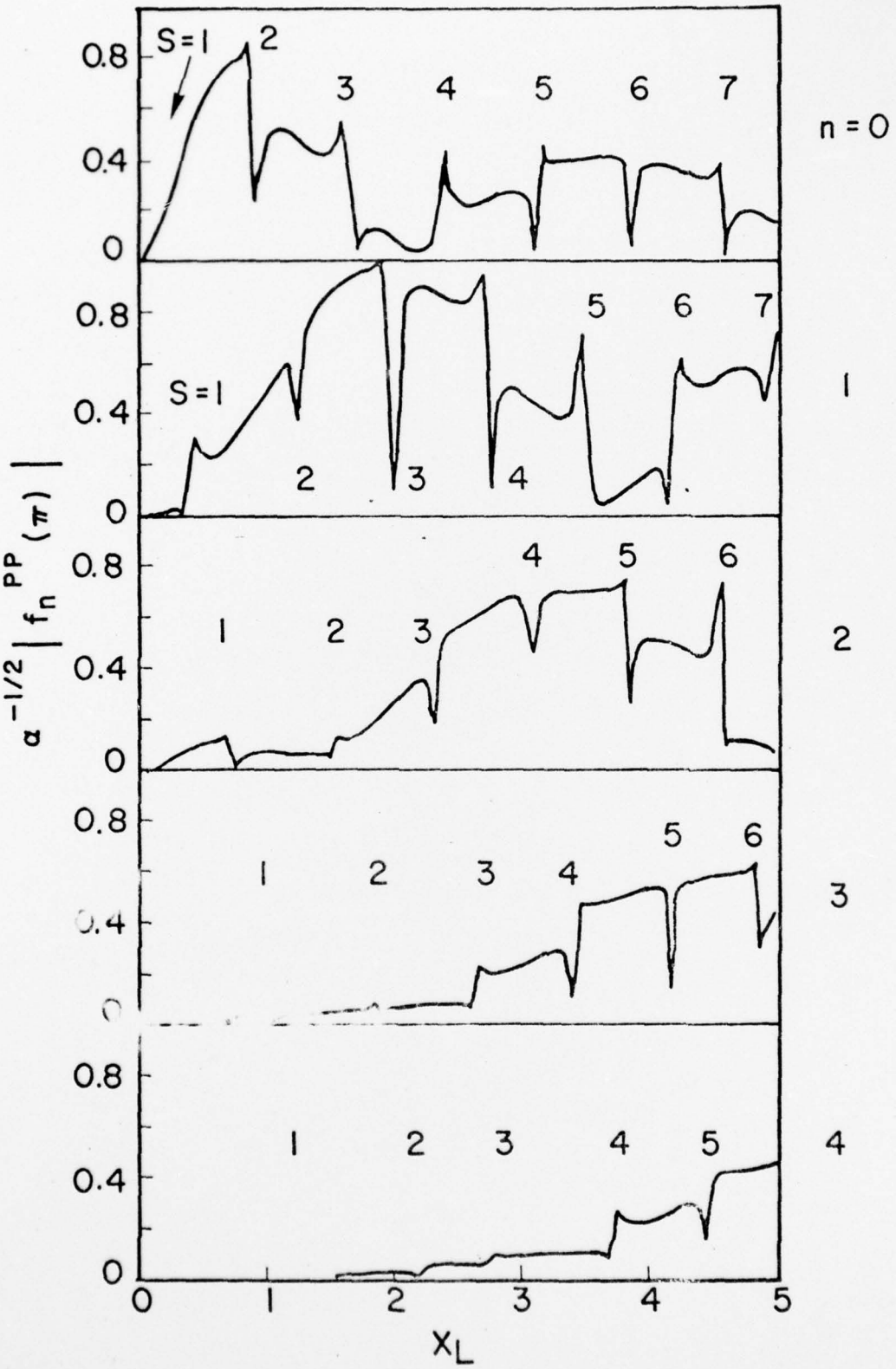

Fig. 9b

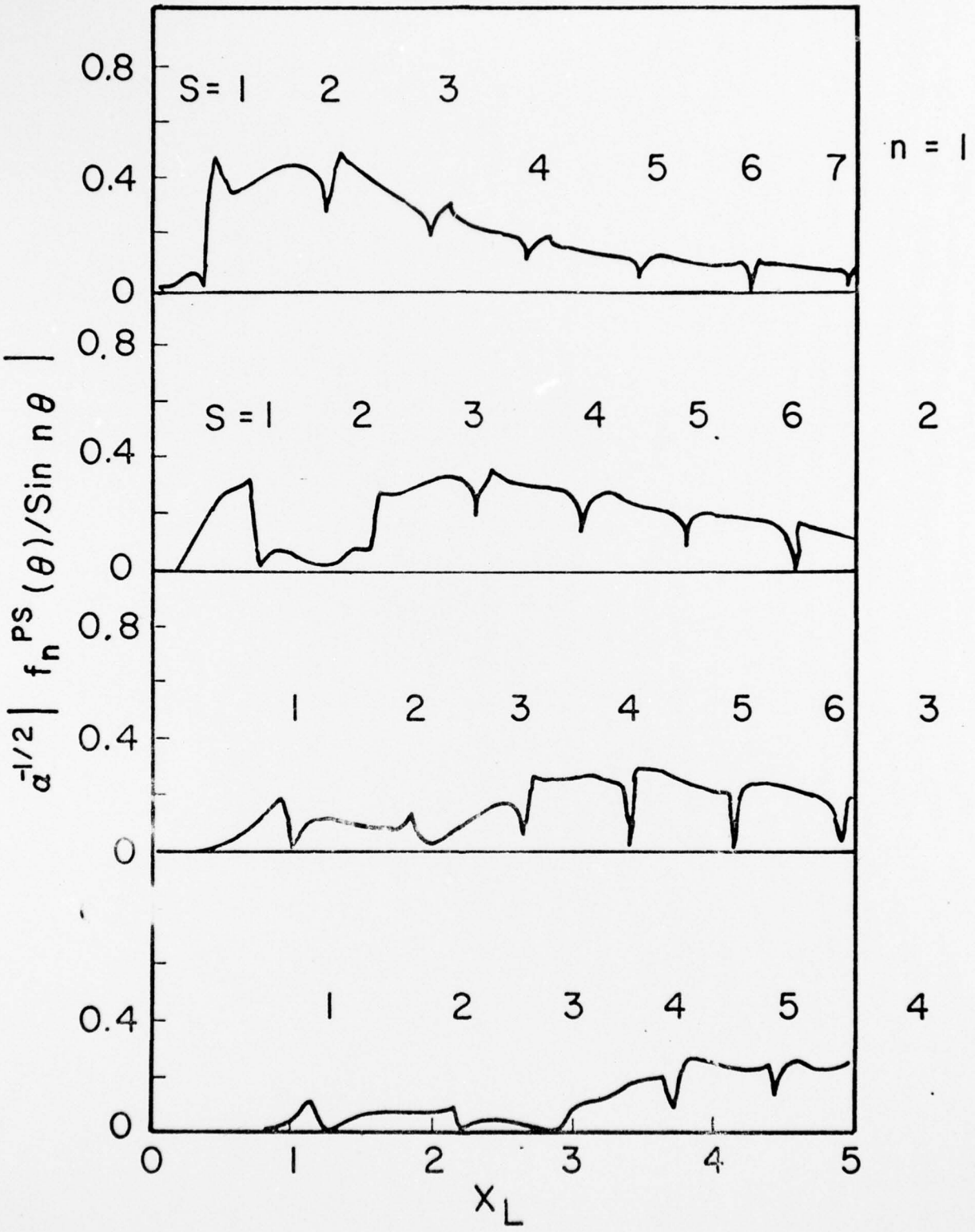
0.8
0.4
0
S= 1 2 3 4 5 6 7
n = 1
S = 1 2 3 4 5 6
2
1 2 3 4 5 6
3
1 2 3 4 5
4
$\alpha^{-1/2} \mid f_n^{PS}(\theta)/\sin n\theta \mid$
0 1 2 3 4 5
X_L

Fig.10a

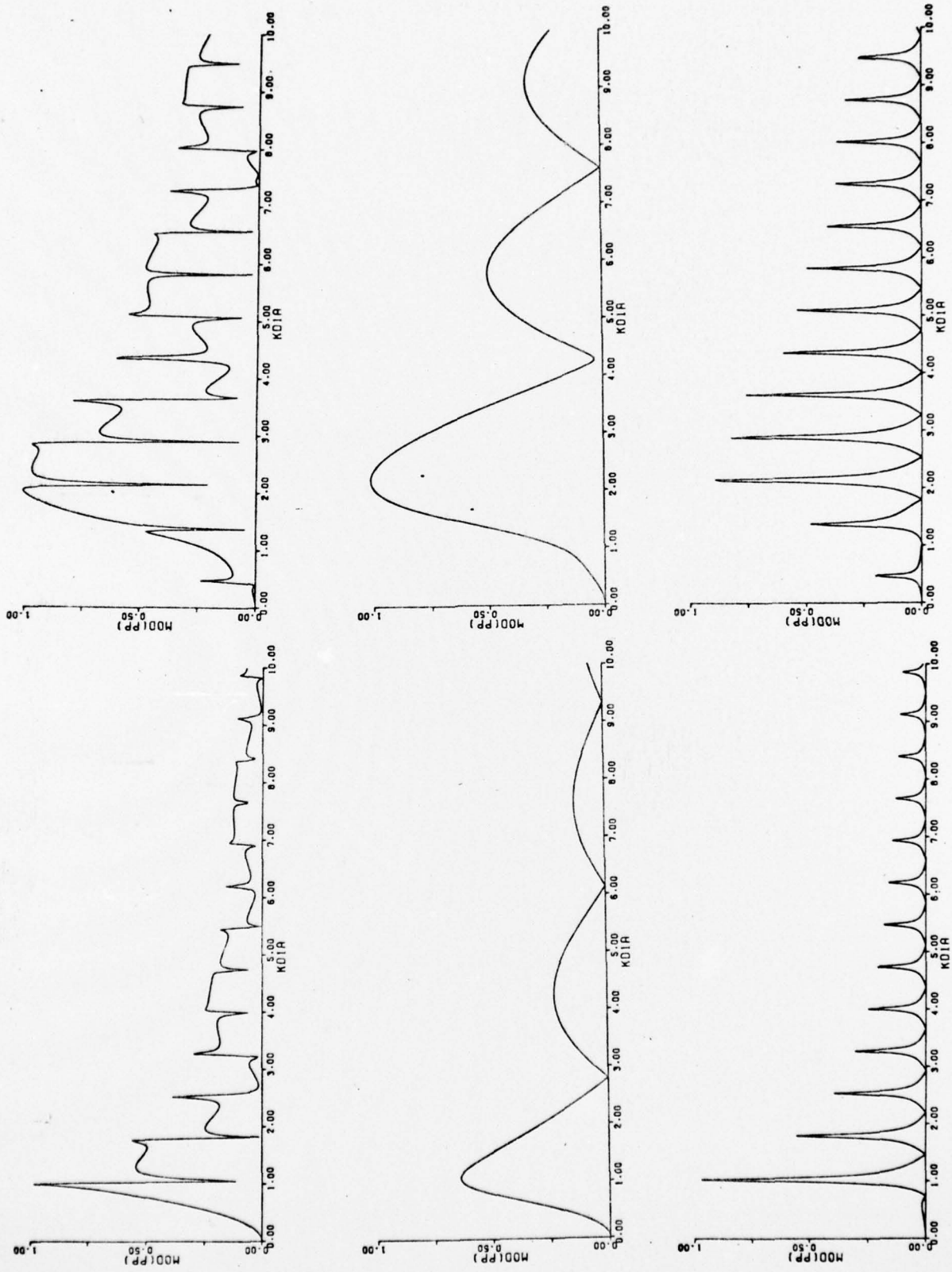

Fig.10b

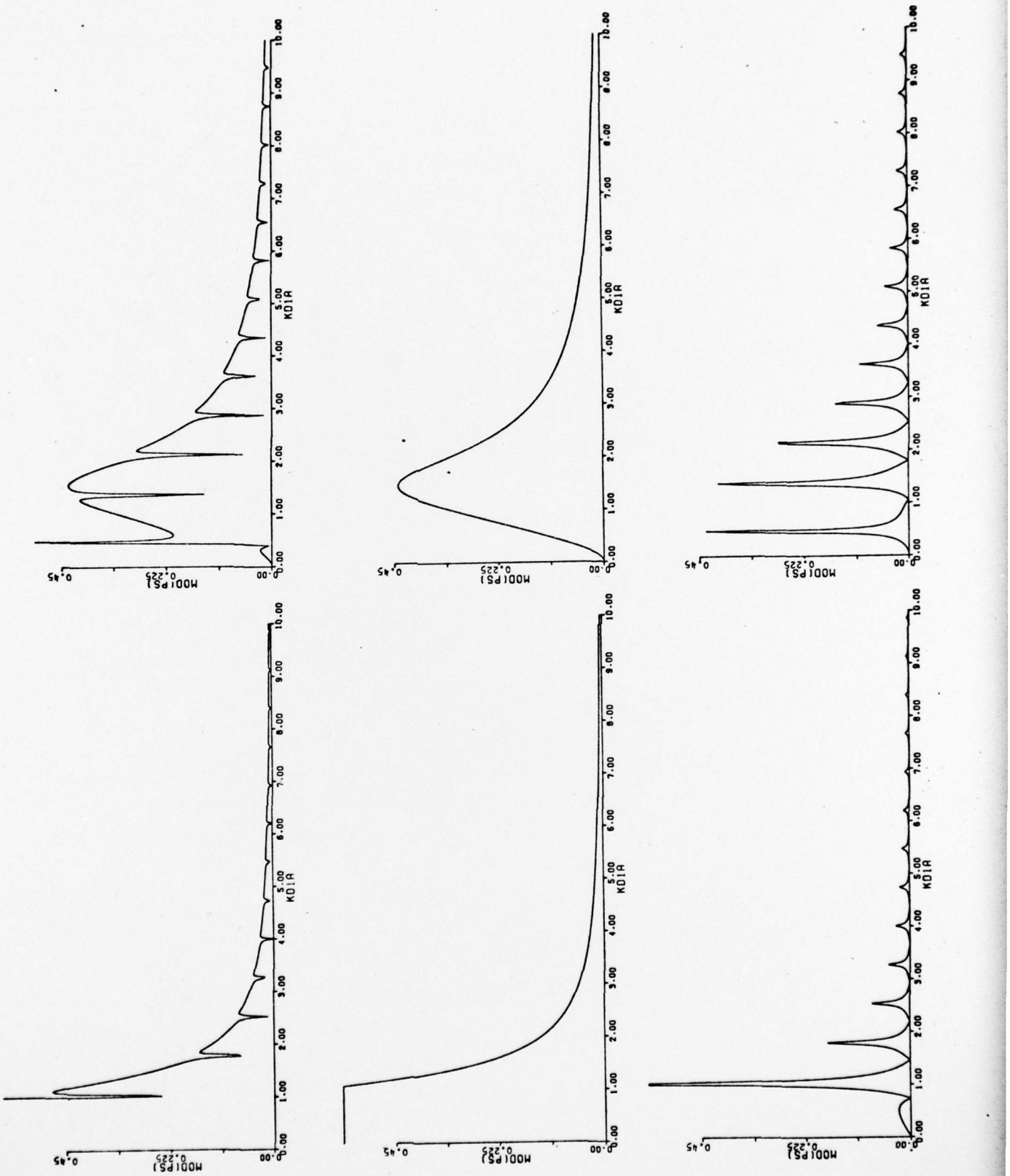
MOD(PSI)
0.45
0.225
0.00
KD1A
0.00
1.00
2.00
3.00
4.00
5.00
6.00
7.00
8.00
9.00
10.00

Fig.10c